

# Uncovering the role of RPL8 in glutathione synthesis-dependent ferroptosis control in hepatocellular carcinoma

Jing Luo<sup>1</sup>, Hao Zhang<sup>1</sup>, Dong Jiang<sup>2</sup>, Yiran Li<sup>2</sup>, Tao Ye<sup>1</sup>

<sup>1</sup>Department of Oncology, Minhang Branch, Zhongshan Hospital, Fudan University, Shanghai, China

<sup>2</sup>Department of Ultrasound, Eastern Hepatobiliary Surgery Hospital, The Third Affiliated Hospital of the Naval Medical University, Shanghai, China

Submitted: 12 April 2024; Accepted: 30 July 2024

Online publication: 5 August 2024

Arch Med Sci

DOI: <https://doi.org/10.5114/aoms/191789>

Copyright © 2024 Termedia & Banach

## Abstract

**Introduction:** Hepatocellular carcinoma (HCC) is significantly impacted by ferroptosis, a form of regulated cell death linked to iron metabolism and oxidative stress. This process is modulated by glutathione (GSH) levels. This study explored the role of ferroptosis-related genes (FRGs) in HCC and evaluated the impact of *RPL8* on HCC progression and ferroptosis mechanisms.

**Material and methods:** Through comprehensive TCGA-LIHC data analysis, we identified significant FRGs affecting HCC prognosis. The expression and functional significance of *RPL8* in HCC were further evaluated using cell line models and tumor xenograft experiments, focusing on its effects on cell proliferation, invasion, migration, apoptosis, and regulation of ferroptosis.

**Results:** Elevated *RPL8* expression was observed in HCC tissues and cell lines. Functional experimental results showed that *RPL8* regulation significantly affects cell proliferation, invasion, migration, and apoptosis. *RPL8* silencing significantly inhibited tumor growth in tumor xenograft experiments. Furthermore, *RPL8* knockdown resulted in increased 4-HNE levels, indicating increased lipid peroxidation and triggering ferroptosis, which was partially alleviated by inhibitors such as Nec-1, Z-VAD-FMK, and Fer-1. *RPL8* was also found to significantly alter the production of glycine, glutamate, and cysteine, upregulate glutathione synthase (GSS) protein levels, and enhance the GSH synthesis pathway.

**Conclusions:** *RPL8* plays a key role in regulating HCC ferroptosis and tumor progression, affecting cellular defense by regulating GSH synthesis. These insights highlight *RPL8* as a promising target for therapeutic intervention in HCC.

**Key words:** hepatocellular carcinoma, ferroptosis, *RPL8*, glutathione, prognostic biomarker.

## Corresponding authors:

Tao Ye  
Department of Oncology  
Minhang Branch  
Zhongshan Hospital  
Fudan University  
200032 Shanghai, China  
E-mail: ye\_tao@fudan.edu.cn

Yiran Li  
Department of Ultrasound  
Eastern Hepatobiliary  
Surgery Hospital  
The Third Affiliated  
Hospital of the  
Naval Medical  
University  
200433 Shanghai, China  
E-mail: liyiranehsh@sina.com

## Introduction

Liver cancer is a typical tumor with significant malignancy, fast growth, and a dismal prognosis [1]. According to the histological criteria, hepatocellular carcinoma (HCC) is usually divided into three types: cholangiocarcinoma, HCC, and mixed liver cancer [2]. Among them, HCC originates from liver parenchymal cells, accounting for about 90% of primary liver cancer, while the latter two types are relatively rare [3]. Generally speak-

ing, in the early stage of the tumor, HCC patients have no obvious clinical signs. However, with the further development of the tumor, there will often be pain in the liver area, decreased appetite, indigestion, nausea, vomiting, weight loss, general weakness, fever, etc., also accompanied by spontaneous hypoglycemia and polycythemia [4]. Currently, medical treatments such as radiotherapy and resection surgery can only relieve pain and extend the survival time of patients [5]. Thus, elucidating the mechanism and finding reliable diagnostic, therapeutic and prognostic biomarkers are indeed critical for HCC patients.

The trace element iron is essential in organismal vitality through its intricate metabolism. This includes systemic processes [6] such as ingested iron absorption by duodenal epithelial cell, peripheral iron circulation via membrane ferroportin, and coupling with transferrin for erythropoiesis, as well as cellular activity such as iron uptake, use, and egress. Notably, dysregulated iron metabolism, manifesting as deficiency [7] or overload [8], disrupts mitochondrial function and cellular integrity. Central to this is ferroptosis [9, 10], the peroxidation of polyunsaturated fatty acid lipids on cell membranes that results in iron-dependent controlled cell death, catalyzed by divalent iron or lipoxygenases. Glutathione (GSH), a crucial antioxidant tripeptide composed of glutamate, cysteine, and glycine, plays a defensive role [11]. It mitigates iron-induced oxidative stress by sequestering free iron, thereby averting ferroptosis. The synthesis of GSH, orchestrated by glutathione synthetase (GSS), is pivotal in converting its constituent amino acids into GSH [12]. Perturbations in iron metabolism and glutathione synthesis are pivotal factors in the complex relationship between iron-mediated cell death and oxidative stress, which may significantly affect cellular functions in HCC.

In the context of HCC, the ribosomal protein L8 gene (*RPL8*), encoding the L8 protein, emerges as a pivotal player with implications for ferroptosis. Recognized as a marker for iron-induced cell death, *RPL8* holds significance in HCC research. Previous investigations identified *RPL8* as one of seven genes associated with ferroptosis, demonstrating its close correlation with survival and treatment responses in gliomas [13]. Moreover, recent findings underscore the impact of *RPL8* on liver cancer progression by modulating the mTORC1 signaling pathway [14]. This emphasizes the integral role of *RPL8* in the intricate process of liver cancer development. Furthermore, elevated *RPL8* expression in liver cancer correlates significantly with adverse prognosis and multiple clinical-pathological parameters [15]. Associations extend to pivotal biological processes such as immune response, liver regeneration, and ferroptosis. These revelations

position *RPL8* as a possible target for therapy for HCC management and a prognostic indicator. In summary, *RPL8* has various roles in ferroptosis, survival, and progression in multiple cancers, emphasizing its critical significance in HCC and its potential for further exploration for effective therapeutic interventions.

This study attempted to elucidate the functional significance of *RPL8* in HCC and its role in the regulation of ferroptosis. First, using public databases, we performed a prognostic evaluation of 22 ferroptosis-related genes (FRGs) in HCC samples. The effects of *RPL8* differential expression on HCC cell growth were subsequently studied through *in vivo* and *in vitro* experiments. Then we further elucidated the relationship between *RPL8* and the ferroptosis mechanism, emphasizing the regulatory effect of *RPL8* on GSH levels and lipid peroxidation. The outcomes of this analysis highlight the relevance of *RPL8* in HCC progression and provide insights into the complex interplay between *RPL8*, GSH metabolism and ferroptosis, with broader implications for cancer treatment and management.

## Material and methods

### Identification and functional analysis of FRGs in liver hepatocellular carcinoma (LIHC)

Utilizing the Assistant for Clinical Transformation website (<https://www.aclbi.com/static/index.html#/>), we analyzed differential expression of 22 FRGs in 371 LIHC samples from The Cancer Genome Atlas (TCGA; <https://tcga-data.nci.nih.gov/tcga/>) database, alongside 226 normal samples from the Genotype-Tissue Expression (GTEx; <https://www.gtexportal.org/home/>) database. Subsequent enrichment analysis for these genes was carried out utilizing the Enrichr website (<https://maayanlab.cloud/Enrichr/>), employing both Gene Ontology (GO) terms and Kyoto Encyclopedia of Genes and Genomes (KEGG) pathways. Additionally, the Search Tool for the Retrieval of Interacting Genes (STRING; <https://string-db.org/>) database was used to conduct protein-protein interaction (PPI) network analysis in order to better understand the interplay of proteins encoded by these genes.

### Progression-free survival (PFS) probability analysis of FRGs

In light of the expression of FRGs, high expression and low expression groups were created out of LIHC patients (both 185 cases) applying the median expression of a gene as the grouping method. The log-rank test was used in the Kaplan-Meier (KM) analysis to compare discrepancies in PFS rates between the two groups. When  $p < 0.05$ , the

prognostic result of FRGs was considered to be statistically significant.

### Construction of risk scores and prognostic model

The glmnet package of R software was used to determine candidate FRGs through the least absolute shrinkage and selection operator (LASSO), and the optimal adjustment parameters ( $\lambda$ ) were determined through ten-fold cross-validation. The patients were categorized into high- and low-risk categories based on their calculated risk ratings. Next, we examined the risk ratings of these groups and analyzed the distribution of survival rates. KM survival curves were plotted to discern differential PFS probabilities between the cohorts, utilizing the log-rank test to determine statistical significance with a  $p$ -value of less than 0.05. For temporal prognostic model validation, the timeROC package was employed at 1-year, 3-year, and 5-year gaps to generate receiver operating characteristic (ROC) curves. Area under the curve (AUC) values were used to evaluate model performance in forecasting the course of survival.

### Prognostic assessment of RPL8 in LIHC

Within our risk prognostic model, RPL8 was established as a hub gene. Univariate and multivariate Cox regression were used in further studies to evaluate the prognostic significance of genes as well as clinical variables such as pT stage, age, and pTNM stage, selecting for variables with significant  $p$ -values. The clinical diagnostic value of RPL8 was then evaluated by ROC curve analysis in the TCGA-LIHC cohort. Furthermore, nomograms for RPL8 in LIHC samples were constructed to forecast the prognosis of the patient at intervals of 1, 3, and 5 years (C-index = 0.59,  $p = 0.001$ ). Calibration plots were generated to represent ideal predictions, providing a visual tool for assessing the accuracy of the prognostic model.

### Expression verification of RPL8

UALCAN (<http://uaHCCan.path.uab.edu/index.html>) is a cancer website for biomarker identification, expression profiling and survival analysis. Here, we examined the RPL8 expression levels across 33 different pan-cancers. Then, correlations between RPL8 expression in LIHC and clinical factors were analyzed, including sample type, individual cancer stage, race, gender, age, and weight.

### Human Protein Atlas (HPA) analysis

The HPA database (<https://www.proteinatlas.org/>) is used to map all human proteins in tissues, organs, and cells. HPA online tools have helped

thousands of researchers in the fields of biomedicine and disease. This study used the HPA database to measure RPL8 protein levels in normal tissues and liver cancer tumor tissues.

### Cell culture

Normal hepatocytes THL-2 and human hepatocellular carcinoma cell lines MHCC-97L, MHCC-97H and SNU387 were provided by the Type Culture Collection Cell Bank (CBTCC, China). High-sugar Dulbecco's Modified Eagle's Medium (DMEM, Gibco, USA) was prepared as the basal medium. 10% fetal bovine serum (FBS) was added to DMEM to provide nutrients required for cell growth. The cell suspension was inoculated into a culture vessel containing the above medium and placed in an incubator at 37°C with 5% CO<sub>2</sub> to maintain the temperature and gaseous environment required for cell growth. When the cells grew to approximately 70–90% density, cell passaging was performed. Cells were detached from the culture vessel using trypsin or non-enzymatic digestion, followed by cell counting and dilution. Depending on the growth of the cells, the medium was changed periodically to remove metabolic waste and provide fresh nutrients. For cells that need to be stored for a long period of time, cryopreservation can be performed. The cell suspension is mixed with the cryopreservation solution and then gradually cooled down to liquid nitrogen for preservation.

### Quantitative real-time polymerase chain reaction (qRT-PCR)

Total RNA was extracted using TRIzol reagent (Ambion, Carlsbad, CA, USA) following the manufacturer's instructions. cDNA synthesis was performed using the PrimeScript RT kit (TaKaRa, Dalian, China). SYBR Green PCR Master Mix (Applied Biosystems, USA) was used on a StepOnePlus real-time PCR system (Applied Biosystems, USA). The total volume of each reaction was 20  $\mu$ l, containing 2  $\mu$ l of cDNA template. Primer sequences are shown below (Table I). Cycling conditions: 5 min of pre-denaturation at 95°C, followed by 40 cycles of 10 s at 95°C, 30 s at 60°C and 30 s at 72°C each. Relative gene expression was subsequently analyzed using the 2- $\Delta\Delta$ CT method with GAPDH as an internal reference. To ensure the stability and reliability of the experimental results and to enhance the statistical validity, we performed more than 3 replications of the biological experiments.

### Cell transfection

We cultivated cells to approximately 70–80% density in preparation for transfection experiments. We calculated the number of cells re-

**Table I.** Sequences of PCR primers used in research to amplify genes

Target	Forward primer (5' to 3')	Reverse primer (5' to 3')
RPL8	TACGCCACCGTTATCTCCCA	CGACCACCACCAGCAACAAC
CBS	CCACACTGCCCCGGCAAAT	CTGGCAATGCCCGTGATGGT
CTH	CAGCAAGACCCGATGCAAAG	CAAAGCAACACCTGCCACTC
SHMT2	CGAGTTGCGATGCTGTACTT	CTGCGTTGCTGTGCTGAG
GSS	CTATGGCAGCTGGTCAAATA	TTCCAAGATCCTGTCCAACAA
GPX4	ATACGCTGAGTGTGGTTTGC	CTTCATCCACTCCACAGCG
GAPDH	CAAGCTCATTCTCTGGTATGAC	CAGTGAGGGTCTCTCTCTCTCT

quired and ensured that each well of the 6-well plate ended up with  $1 \times 10^5$  cells/well. We spread the cells into 6-well plates at a density of  $1 \times 10^5$  cells/well using aseptic manipulation. The cells were cultured overnight until the cells adhered. We purchased siRNA transfection reagents targeting the RPL8 gene from Polyplus. We diluted the siRNA transfection reagent with serum-free medium according to the reagent instructions to avoid the effect of serum on transfection efficiency. On the day of transfection, we mixed the siRNA transfection reagent with cell culture medium to ensure that the siRNA was fully bound to the transfection reagent. The mixed siRNA transfection complex was added to each well, usually with a volume of 2–3 ml per well. Plasmids containing the RPL8 gene were purchased from Obio. We diluted the RPL8 plasmid with serum-free medium according to the experimental design. We added the mixture of RPL8 plasmid and transfection reagents to the target wells and set up a control with an empty vector (empty vector). We ensured that the volume of transfection complex in each well was 2–3 ml. We returned the 6-well plate to the incubator and continued incubation for 24–48 h to ensure siRNA and plasmid expression.

#### Cell viability assay

$1 \times 10^5$  cells/well were grown in 6-well plates containing culture medium, and the cells were placed in an incubator for 24 h. Subsequently, the cells were treated with trypsin (trypsin) to detach them from the 6-well plate. The cells were suspended and counted, the cell concentration was adjusted, and the cells were dispensed into 96-well plates, with the same number of cells added to each well, and double spreading was performed to ensure the reproducibility of the experiment. 10  $\mu$ l of CCK-8 solution (Cell Counting Kit-8, SAB Biotech, USA) was added to each well of the 96-well plate for 4 consecutive days to ensure even distribution of CCK-8 solution in each well. The 96-well plate was incubated in an incubator to allow CCK-8 to react with metabolically active substances in the cells. The absorbance (OD) of

each well was measured at different time points using an enzyme marker (microplate reader), with the wavelength usually set at 450 nm. The OD value of each measurement was recorded.

#### Transwell assays

We prepared the Transwell chambers by ensuring that they were clean and suitable for experimental use by pre-coating the filter membrane of the Transwell chambers with an appropriate amount of Matrigel Matrix Gel. Tumor cells were counted and adjusted to a concentration of  $1 \times 10^6$  cells/ml and added to the upper chamber of the Transwell. Culture medium containing 20% FBS was added to the lower vessel of the Transwell chambers, and the Transwell chambers were incubated in an incubator for 24 h. Subsequently, the medium was removed from the lower container of the Transwell chambers. The lower vessel of the Transwell chambers was washed twice using PBS to remove non-migrating or non-invasive cells. Cells on the filter membrane were fixed using methanol at room temperature for 5 min. The fixed filter membrane was allowed to dry at room temperature for approximately 30 min. The cells were stained using DAPI staining solution for 20 min. The stained filter membrane was placed on a microscope slide, and a fluorescence microscope was used to observe the cells at 200 $\times$  magnification and take pictures of the migrated and invaded areas of the cells on the filter membrane. The pictures taken were analyzed using ImageJ software to calculate the gray scale values of the migrated and invaded cells and to assess the migratory and invasive abilities of the cells.

#### *In vivo* tumorigenesis assay

The Animal Center of the Chinese Academy of Medical Sciences (Beijing, China) supplied eight BALB/c nude mice (5 weeks old, male) for xenotransplantation experiments. Subcutaneous injections of MHCC-97 cells into the armpits of nude mice were performed, with non-targeted siRNA-treated (si-NC) cells serving as the negative control group and those transfected with si-

RPL8 as the experimental group, each consisting of four mice. A vernier caliper was used every 5 days to measure the volume of the tumor in mice. Mice were sacrificed 6 weeks after injection to observe tumors. The Medical Ethics Committee of the Third Affiliated Hospital of the Naval Medical University gave its approval before this study could begin, guaranteeing that ethical standards for the humane treatment of research animals were followed. Ethical approval number: EHBH-KY2021-K-011; ethical approval date: 06/04/2021.

#### Enzyme-linked immunosorbent assay (ELISA) and metabolite measurements

Lichen Biotech Ltd. provided ELISA kits to detect RPL8, glutamate, glycine, cystathionine, cysteine, glucose, and serine (Shanghai, China). The relation between RPL8 and labile iron was measured using Abcam kits (Cambridge, UK), while GSH and membrane phospholipid levels were detected by Sigma kits (St. Louis, MO, USA). The ELISA was performed strictly according to instructions provided by the manufacturer.

#### Western blotting (WB)

Cellular proteins were extracted using RIPA lysis buffer (Thermo Fisher Scientific) and protein concentration was determined using BCA assay (Thermo Fisher Scientific). Aliquots of protein samples were electrophoresed on 10% SDS-PAGE gels. Wet transfer was performed using a PVDF membrane (MilliporeSigma) with a membrane transfer time of 60 min at a constant flow of 0.3 A. Membranes were closed using 5% skimmed milk powder in TBST for 2 h, followed by overnight incubation at 4°C with primary antibodies (RPL8, Bax, Bcl-2, cleaved caspase-3, GPX4, CBS, CTH, SHMT2, GSS etc.). In the experiments, Bcl-2 and SHMT2 were diluted at 1 : 2000 and the rest at 1 : 1000. GAPDH (1 : 5000) was used as an internal control. This was followed by incubation for 1 h at room temperature using HRP-labelled secondary antibodies. The bands were visualized using an electrochemiluminescence (ECL) detection system (Thermo Fisher Scientific) and densitometry was performed for quantification. To ensure the stability and reliability of the experimental results, each biological experiment was repeated more than three times.

#### Flow cytometry apoptosis assay

Flow cytometry was used to quantify apoptotic cells after labeling with Annexin V-FITC and propidium iodide (PI) with the FITC Annexin V Apoptosis Detection Kit I (BD Biosciences). Following cell collection, two cold PBS washes and a resuspension in 1X binding buffer were performed. Following

that, cells were treated in the dark for 15 min with Annexin V-FITC and PI. After incubation, samples were analyzed using a BD Biosciences FACSCalibur flow cytometer to determine the proportion of apoptotic cells. Data were then processed using CellQuest software.

#### Statistical analysis

All experiments had at least three biological replicates. Each biological replicate was performed and analyzed independently to ensure reproducibility and accuracy. For *in vitro* experiments (cell proliferation, migration, invasion), there were three technical replicates for each biological replicate in each condition. For *in vivo* studies, a minimum of four mice per group was used to ensure adequate statistical power.

All analyses involving statistics were performed using SPSS 18.0 software (SPSS Inc.), data are expressed as mean  $\pm$  standard deviation (SD), comparisons between two groups were performed using Student's *t*-test, and statistical significance was set at  $p < 0.05$ , with *p*-values expressed as follows:  $p < 0.05$  (\*),  $p < 0.01$  (\*\*).

## Results

### Functional enrichment and prognostic evaluation of FRGs in LIHC

Twenty-two FRGs were differentially expressed in TCGA-LIHC samples, as shown in Figure 1 A. Subsequent KEGG analysis showed the enrichment of these genes, including ferroptosis, thyroid cancer, central carbon metabolism in cancer, etc. (Figure 1 B). Within the GO terms, the FRGs were predominantly enriched in processes such as long-chain fatty acid metabolic process, PERK-mediated unfolded protein response, etc. (Figure 1 C). Further PPI analysis was conducted on the 22 differentially expressed FRGs, revealing potential interplay among these genes (Figure 1 D). Finally, survival analysis identified 6 FRGs (*SLC7A11*, *TFRC*, *CISD1*, *CS*, *FANCD2*, *RPL8*) that were significantly correlated with the outcome of HCC patients, and elevated expression of these 6 genes was associated with a lower chance of PFS in patients (Figures 1 E–J).

### Analysis of the prognostic ability of 4 FRGs in the risk model in LIHC

LASSO Cox regression analysis was employed to construct an ideal gene signature from 6 FRGs, with the gene *CS* not showing significant results (Figures 2 A, B). The 10-fold cross-validation method identified four genes (*SLC7A11*, *FANCD2*, *CISD1*, and *RPL8*) in the risk score model construction. In the risk model, higher risk scores were associated

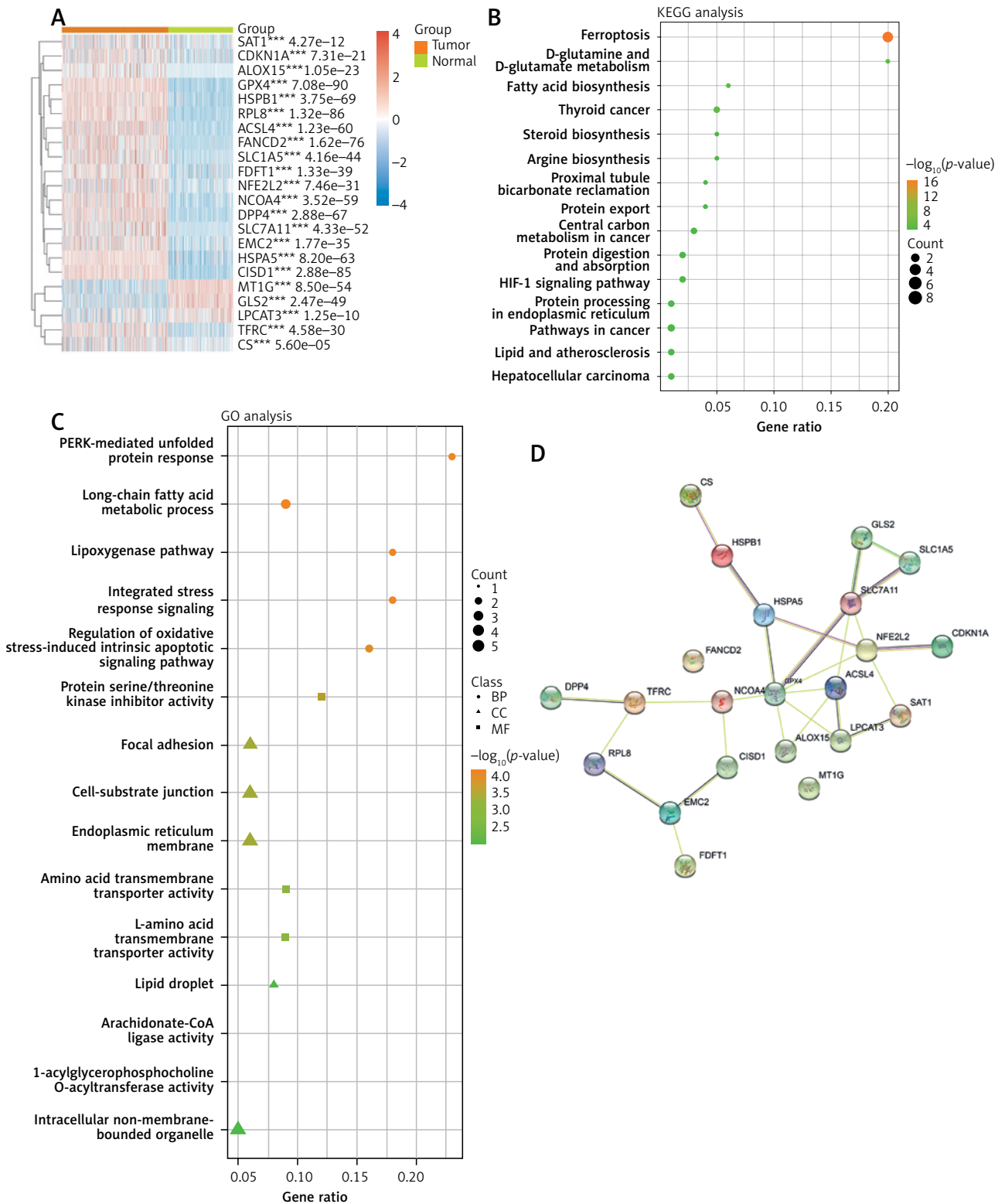


**Figure 1.** Differential expression, functional enrichment and survival analysis of FRGs in LIHC. **A** – The heatmap illustrates the manifestation patterns of 22 FRGs in both normal and tumor tissues. The color scale, located in the upper right corner, indicates expression levels, with red representing high expression and blue representing low expression. **B, C** – Scatter plots depict the findings of KEGG pathway (**B**) and GO term enrichment analysis for FRGs. The y-axis displays the enriched KEGG pathways or GO terms, and the x-axis shows the gene ratio. The size of each data point corresponds to the number of FRGs within each KEGG pathway or GO term. The size of each dot represents the number of genes associated with each term, with colors indicating the significance level ( $p$ -value). **D** – The PPI network analysis represents interactions among FRG-encoded proteins or protein domains

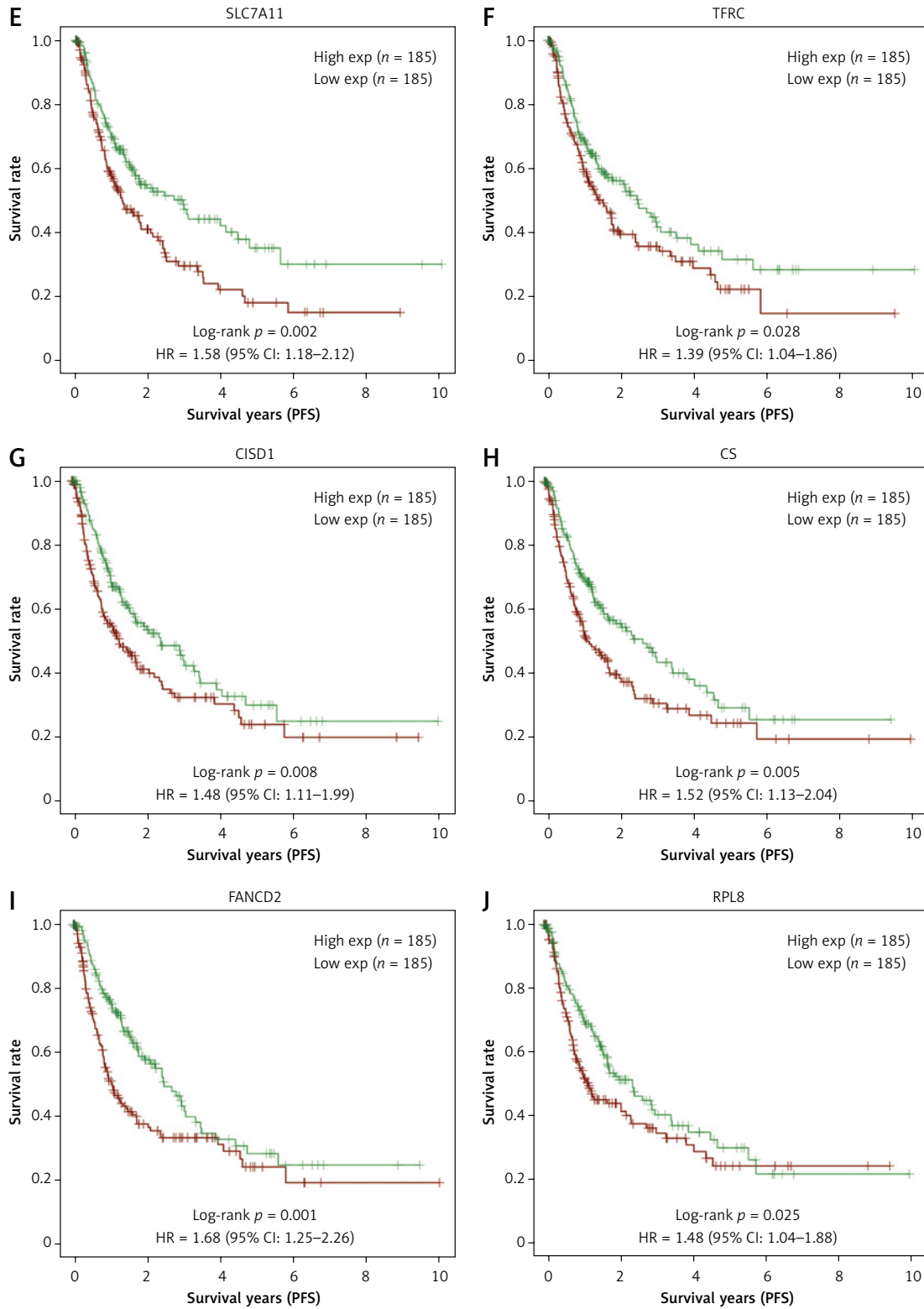
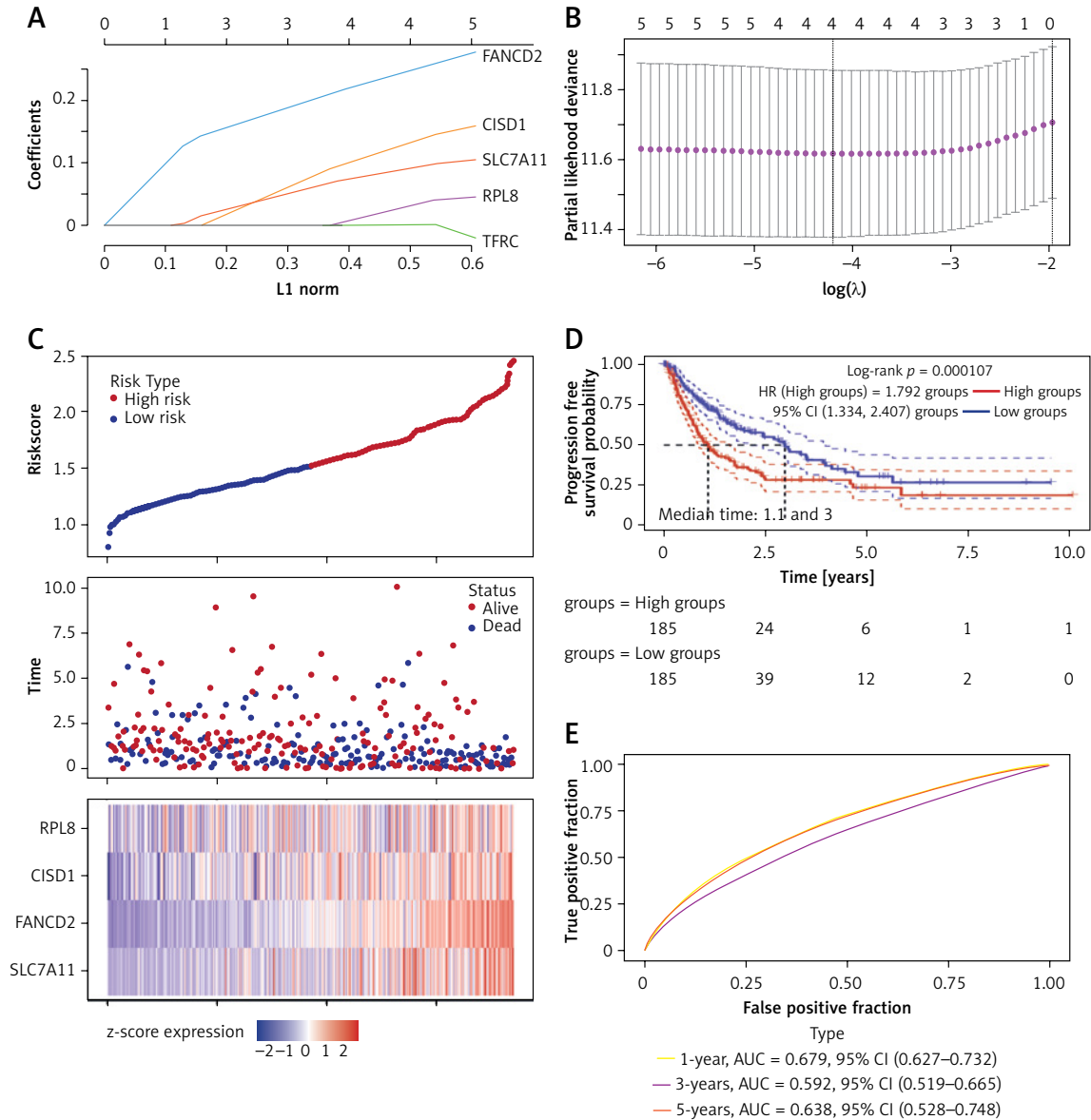


Figure 1. Cont. E–J – Batch PFS survival analysis of *SLC7A11*, *TFRC*, *CISD1*, *CS*, *FANCD2* and *RPL8*, respectively



**Figure 2.** LASSO and risk score analyses of FRGs. **A** – The coefficient spectrum obtained through LASSO regression analysis for FRGs. Each line represents a gene. **B** – Tenfold cross-validation for LASSO regression to determine the optimal lambda ( $\lambda$ ) value. Red dots represent the partial likelihood deviance for different values of  $\log(\lambda)$ , while the gray lines denote the standard error. The vertical dotted lines indicate the lambda values with minimum error and one standard error from the minimum. **C** – Risk score analysis and patient survival status. The upper panel shows the distribution of risk scores for patients classified into high-risk and low-risk groups. The middle panel depicts the survival status of patients, with red dots indicating deceased patients and blue dots indicating alive patients. The lower panel presents a heatmap of the expression profiles for the four prognostic genes (*RPL8*, *CISD1*, *FANCD2*, *SLC7A11*), with color gradients representing the z-score of expression levels. **D** – The survival curves represent Kaplan-Meier analysis for the four prognostic genes. The x-axis denotes time in years, and the y-axis indicates PFS probability. **E** – ROC curves of the risk model in 1 year, 3 years and 5 years. The curves in different colors represent the AUC values in different time periods

with shorter survival and increased mortality in high-risk patient groups. Notably, the expression of these four genes also showed significant differences (Figure 2 C). Individuals in the high-risk category had significantly shorter PFS than those in the low-risk category, according to subsequent KM survival curves ( $p = 0.000107$ ) (Figure 2 D). Additionally, the ROC curve study demonstrated the precision of the risk model in forecasting PFS

over 1, 3, and 5 years, emphasizing its potential clinical application (Figure 2 E).

### Construction of predictive nomogram of *RPL8* in HCC prognosis

After analysis by univariate and multivariate Cox regression, *RPL8* was determined as a separate predictor of the prognosis of HCC (Figures 3 A, B). The ROC curve indicated that *RPL8* had a better

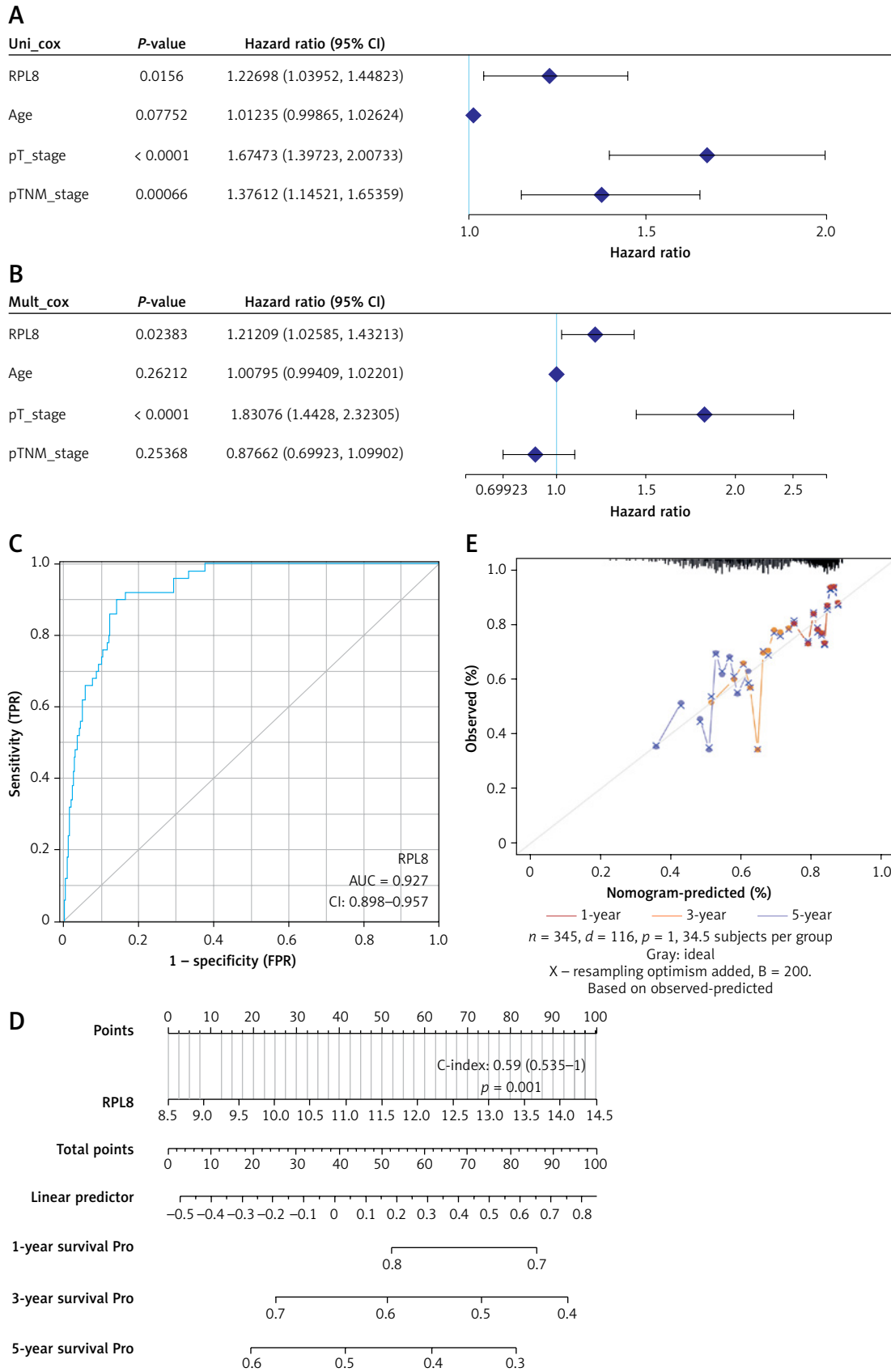


**Figure 3.** Prognostic nomogram analysis of *RPL8* in HCC. **A, B** – Results of univariate and multivariate Cox regression analyses, respectively, assessing the prognostic significance of *RPL8* in HCC. **C** – The ROC curve illustrates the analysis of *RPL8* predictive power for HCC prognosis. **D** – The nomogram generates predictive calibration plots for 1-year, 3-year, and 5-year OS rates in HCC patients. **E** – Calibration curves compare predicted and actual survival outcomes, highlighting the robust predictive performance of the model for 1-year, 3-year, and 5-year OS in HCC patients

prognosis prediction effect in HCC (Figure 3 C). As shown in Figure 3 D, the 1-, 3-, and 5-year survival possibilities of HCC individuals were anticipated by the nomogram. Next, utilizing the calibration curve, the generated nomogram's prediction accuracy was confirmed, as shown in Figure 3 E.

### Correlation analysis between *RPL8* levels and different clinical parameters of LIHC

We examined *RPL8* expression patterns across 33 cancer types to learn more about *RPL8* in other malignancies. When compared to normal tissues from the same organs, *RPL8* was found to be higher in most tumor tissues (Figure 4 A), suggesting its potential involvement in tumorigenesis. Subsequently, we investigated the association between *RPL8* expression and the clinicopathological traits

of LIHC. In primary tumors, *RPL8* expression was higher than adjacent non-tumorous tissues (Figure 4 B). Significant variations in *RPL8* expression were evident across different demographic and physiological groups: Caucasian versus Asian, African American versus Asian, and patients aged 41–60 years versus those 81–100 years, as well as between extreme weight and obese (Figures 4 D, F, G). However, no significant differences were observed in *RPL8* expression according to individual cancer stages or patient's gender (Figures 4 C, E).

### *RPL8* regulates malignant growth of HCC cells *in vivo* and *in vitro*

Analysis of the HPA database revealed elevated levels of *RPL8* protein in HCC tissues in contrast to normal liver tissues (Figure 5 A). Furthermore,

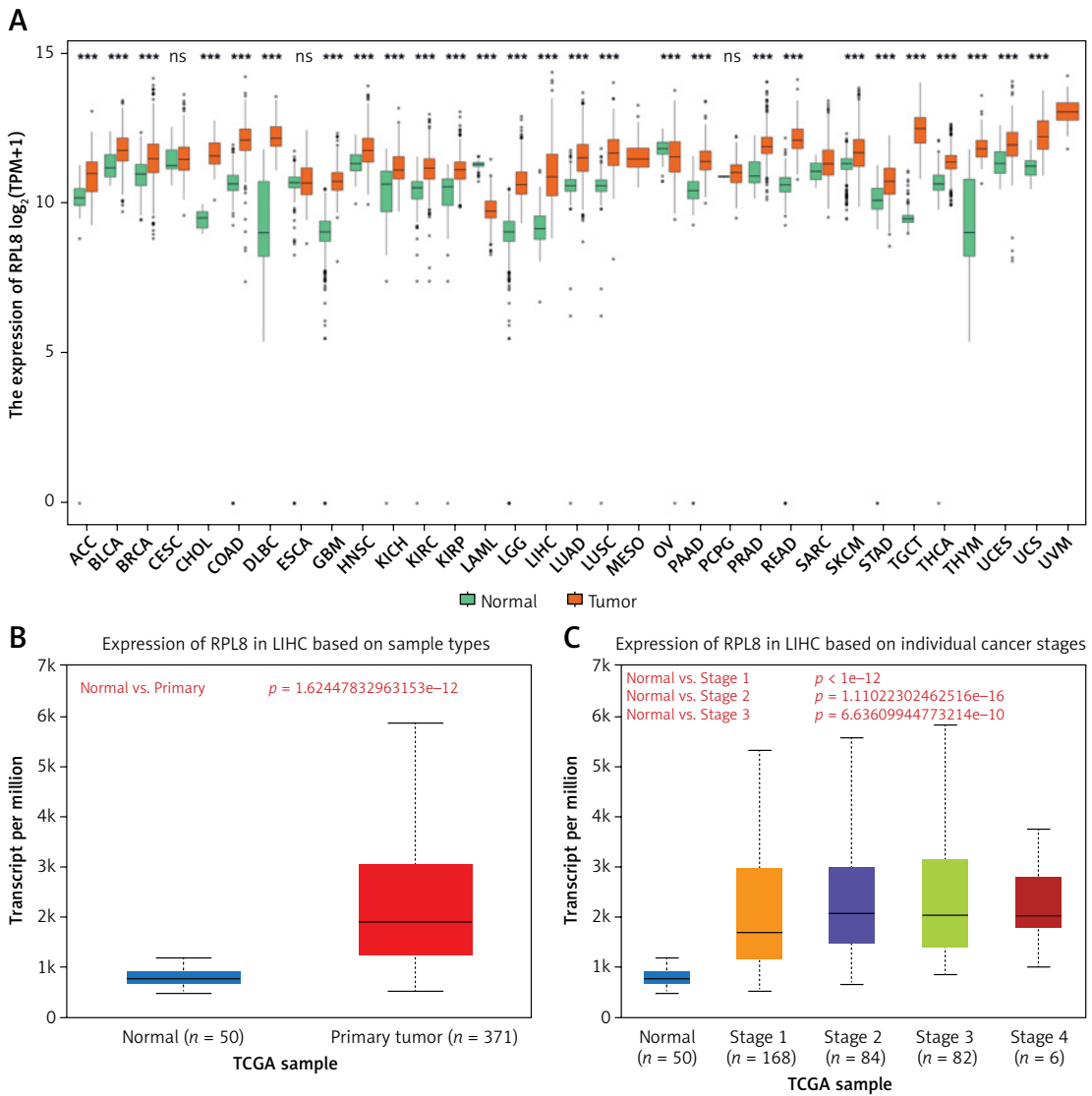


**Figure 4.** Expression analysis of *RPL8* in UALCAN database. **A** – The boxplot illustrates the comparison of *RPL8* expression levels in pan-cancers. The x-axis represents 33 cancer types. Gene expression levels are displayed on the y-axis, with red indicating tumor tissues and green representing normal tissues. **B–C** – Boxplots depict *RPL8* expression in TCGA-LIHC specimens based on different sample types (**B**), individual cancer stages (**C**). \*\*\* $P < 0.01$ , ns means not significant

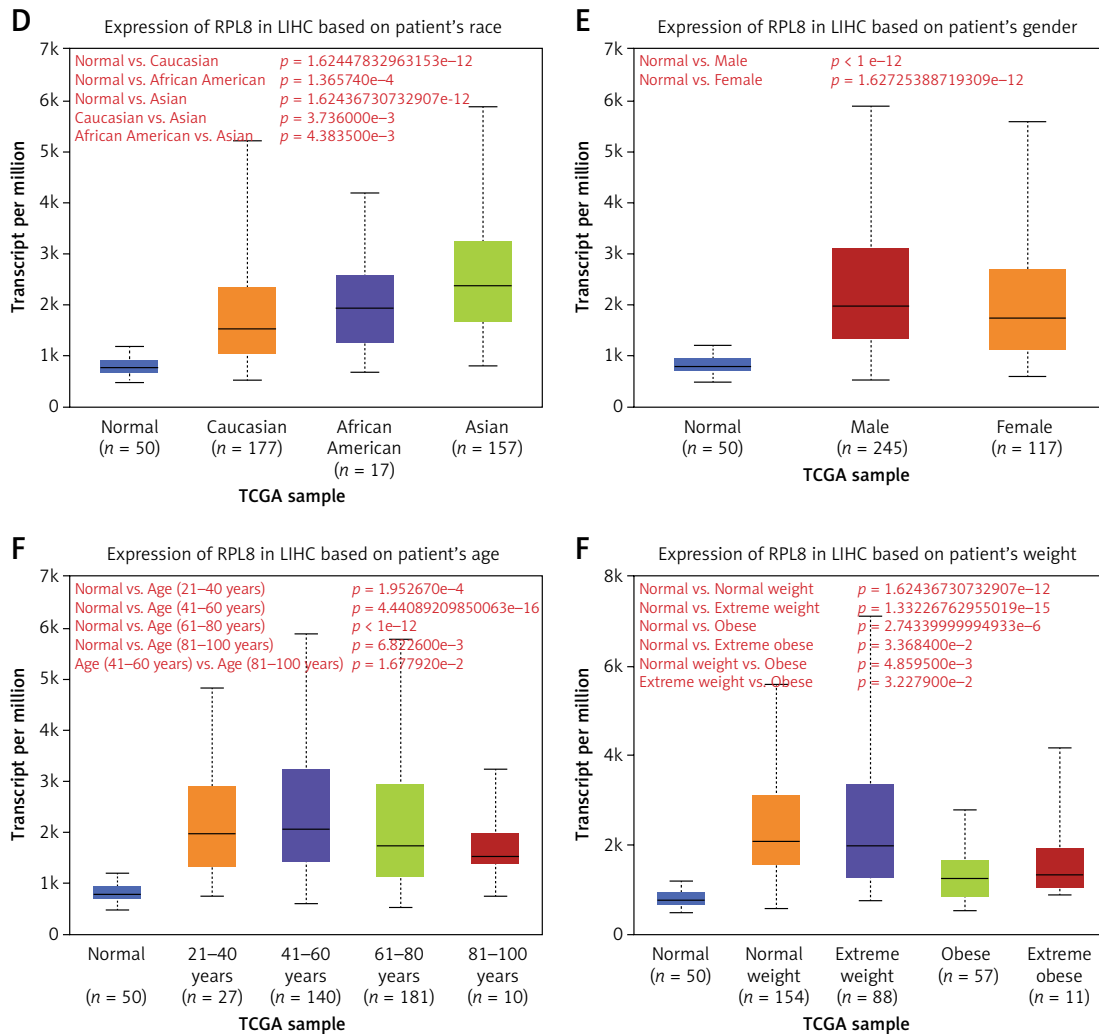


**Figure 4.** Cont. D–G – race (D), gender (E), age (F), and weight groups (G), respectively. \*\*\* $P < 0.01$ , ns means not significant

RPL8 was found to have elevated mRNA and protein levels in HCC cell lines, especially in MHCC-97H and SNU387 cells (Figure 5 B). Therefore, these two cell lines were used for subsequent experimental analyses. RPL8 expression was successfully knocked down and overexpressed in MHCC-97H and SNU387 cells, respectively, with significant efficiency (Figures 5 C and 5 F). *In vitro* experiments showed that RPL8 knockdown can dramatically reduce the migration, invasion, and proliferation of cells (Figures 5 D, E, 6 A–D). In contrast, RPL8 overexpression promoted these processes (Figures 5 G, H, 6 E–H). Importantly, overexpression of RPL8 in knockout models partially or completely rescued the observed phenotype in knockout models, highlighting the potential therapeutic importance of RPL8 in HCC treatment strategies (Figure 7). Mouse xenograft experiments showed that tumor size and volume were reduced after RPL8 knockdown (Figures 6 I, J). In addition, through flow cytometry and WB experiments (Figures 8 A–F), silencing RPL8 was noted

to enhance apoptosis in HCC cells, indicated by reduced Bcl-2 expression and elevated levels of the pro-apoptotic proteins cleaved caspase-3 and Bax. Overexpression of RPL8 produced the opposite effect. Our results validated that RPL8 can serve as a key regulator of HCC progression and participate in the regulation of cell behaviors related to tumor development *in vivo* and *in vitro*.

#### RPL8 influences ferroptosis by regulating GSH in HCC

The levels of 4-hydroxynonenal (4-HNE) increased after RPL8 knockdown compared with overexpression. The increase in 4-HNE induced by RPL8 silencing could be partially reversed by the necrosis inhibitor necrostatin-1 (Nec-1), the ferroptosis inhibitor ferrostatin-1 (Fer-1), and the apoptosis inhibitor Z-VAD-FMK (Figure 9 A). These results indicate that RPL8 regulates 4-HNE production and that its knockdown leads to enhanced lipid peroxidation that can be alleviated by specific pathway inhibitors. Previous studies

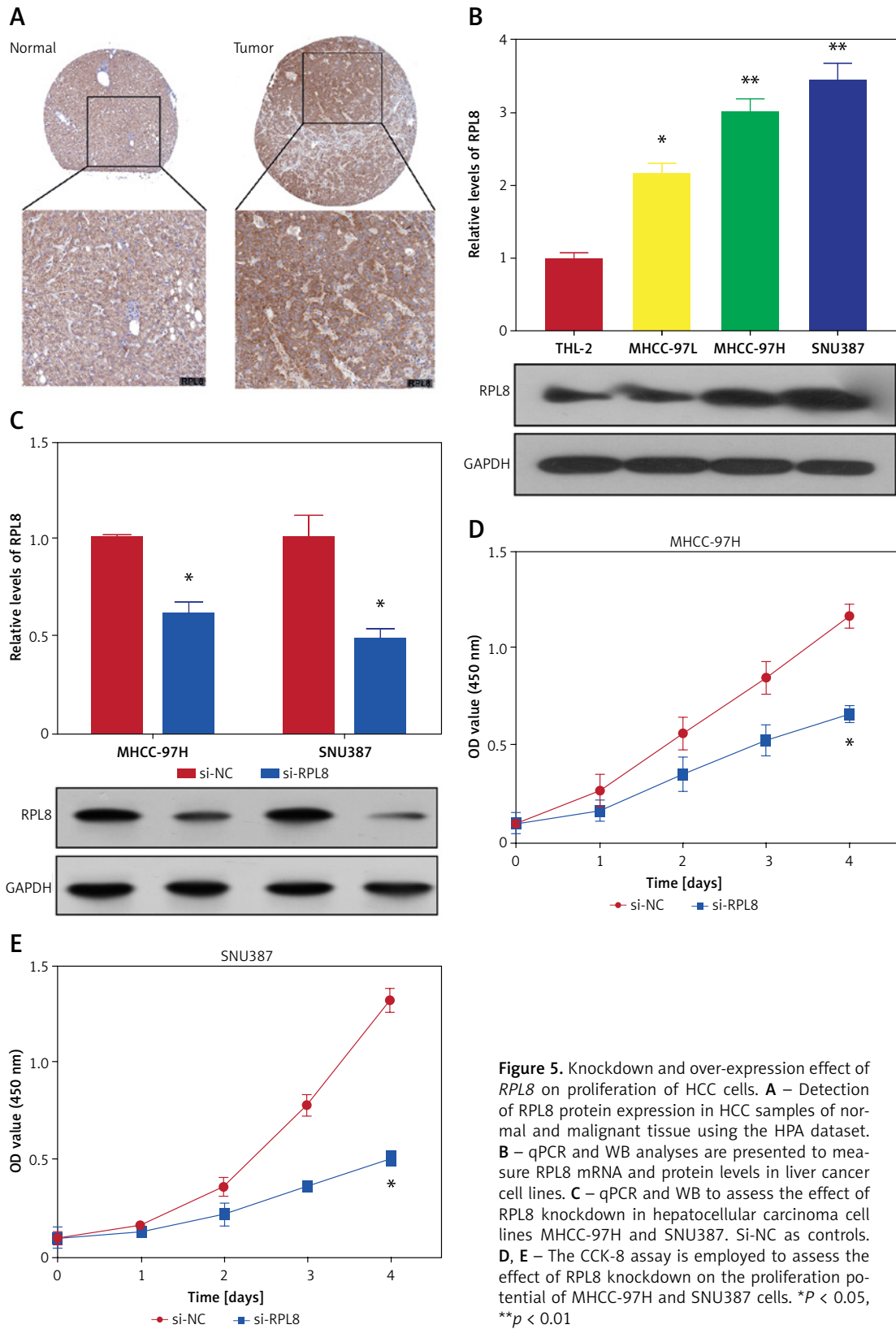


**Figure 5.** Knockdown and over-expression effect of *RPL8* on proliferation of HCC cells. **A** – Detection of *RPL8* protein expression in HCC samples of normal and malignant tissue using the HPA dataset. **B** – qPCR and WB analyses are presented to measure *RPL8* mRNA and protein levels in liver cancer cell lines. **C** – qPCR and WB to assess the effect of *RPL8* knockdown in hepatocellular carcinoma cell lines MHCC-97H and SNU387. Si-NC as controls. **D, E** – The CCK-8 assay is employed to assess the effect of *RPL8* knockdown on the proliferation potential of MHCC-97H and SNU387 cells. \* $P < 0.05$ , \*\* $p < 0.01$

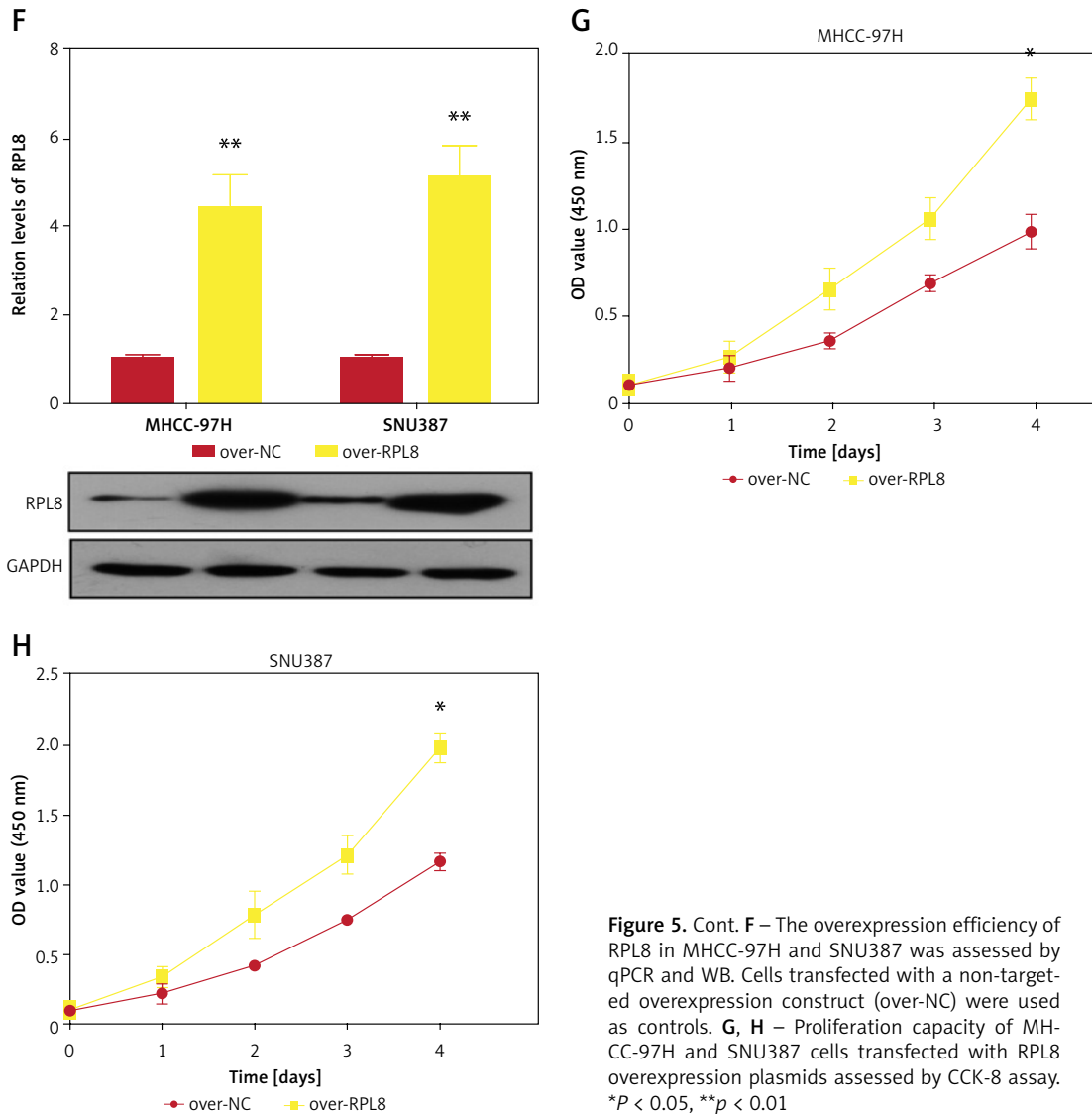


**Figure 5.** Cont. **F** – The overexpression efficiency of RPL8 in MHCC-97H and SNU387 was assessed by qPCR and WB. Cells transfected with a non-targeted overexpression construct (over-NC) were used as controls. **G, H** – Proliferation capacity of MHCC-97H and SNU387 cells transfected with RPL8 overexpression plasmids assessed by CCK-8 assay. \* $P < 0.05$ , \*\* $p < 0.01$

have suggested that the accumulation of lipid reactive oxygen species (ROS) is the last stage of the ferroptosis induction process, and that its production is at least controlled by phospholipids, labile iron, and glutathione [16]. Furthermore, our study revealed that GSH levels are positively regulated by *RPL8*, while labile iron and membrane phospholipid levels remain unchanged (Figures 9 B–D), indicating that *RPL8* may inhibit ferroptosis by elevating GSH levels, thus providing a protective mechanism against lipid peroxidation and cell death.

#### *RPL8* regulates the ferroptosis-related metabolic axis in HCC

Figure 10 A shows the metabolic pathway of glucose into serine, which is further processed into glycine and cystathionine, both precursors for GSH synthesis [17]. This process is critical for the regulation of ferroptosis, in which GSH and

*GPX4* enzymes play key protective roles [18]. An ELISA assay was used to evaluate the levels of key biochemical molecules involved in GSH synthesis and metabolism before and after regulation of *RPL8* expression in HCC. As demonstrated in Figures 10 B–G, overexpression of *RPL8* remarkably reduced the levels of glycine, glutamate, and cysteine, while knockdown of *RPL8* resulted in an increase in these factors, indicating that *RPL8* enhances GSH synthesis to stimulate GSH synthesis. In contrast, the production of cystathionine, serine, and glucose was not affected by *RPL8*. Subsequent research focused on enzymes involved in GSH metabolism, including cystathionine- $\beta$ -synthase (*CBS*), serine hydroxymethyltransferase 2 (*SHMT2*), cystathionine- $\gamma$ -lyase (*CTH*), *GSS* and *GPX4*. According to the results, *RPL8* did not show significant regulatory effects on *CBS*, *SHMT2*, *CTH* and *GPX4*. However, it positively regulated the protein levels of *GSS* (Figures 10 H–K). This highlights the specific regulatory role of *RPL8* in enhancing

GSH synthesis by upregulating GSS, which may contribute to the mechanisms of cellular defense against oxidative stress and ferroptosis.

### Discussion

HCC is an aggressive tumor that poses a significant threat to human life. The early symptoms

of HCC are not apparent, which makes it more difficult to diagnose. When symptoms such as liver pain, weight loss, and abdominal mass occur, HCC has often progressed to the middle and late stages. Advanced HCC is often accompanied by a series of complications, such as hepatic encephalopathy, upper gastrointestinal bleeding, and

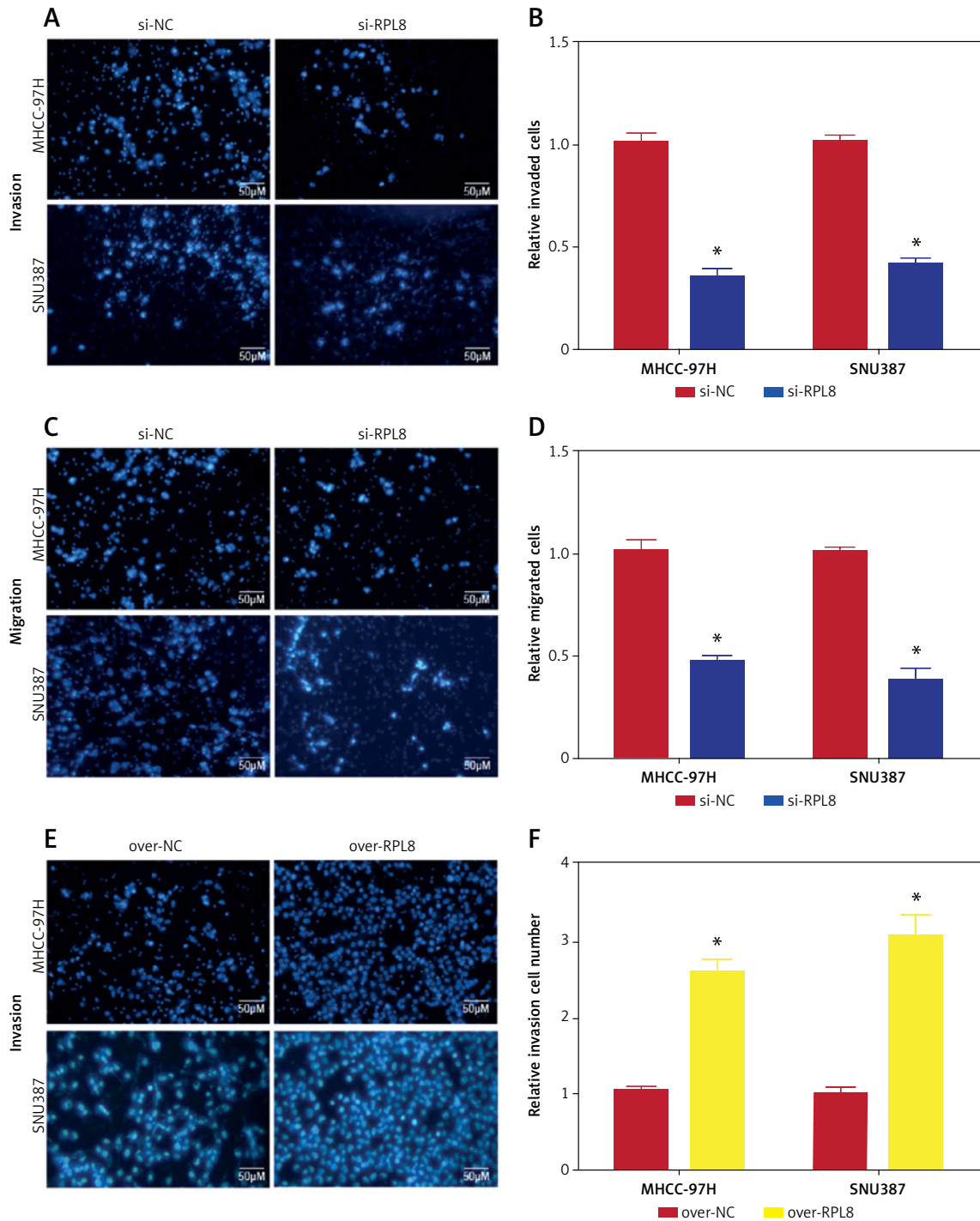


**Figure 6.** Impacts of *RPL8* modulation on invasion, migration, and *in vivo* tumor growth in HCC cells. **A–D** – Transwell assays evaluating the impact of *RPL8* knockdown on invasion (**A, B**) and migration (**C, D**) in MHCC-97H and SNU387 cells. Si-NC as controls. **E–F** – Transwell assays assessing the impact of *RPL8* overexpression on invasion (**E, F**). Scale bars: 50  $\mu$ m, \* $p$  < 0.05, \*\* $p$  < 0.01

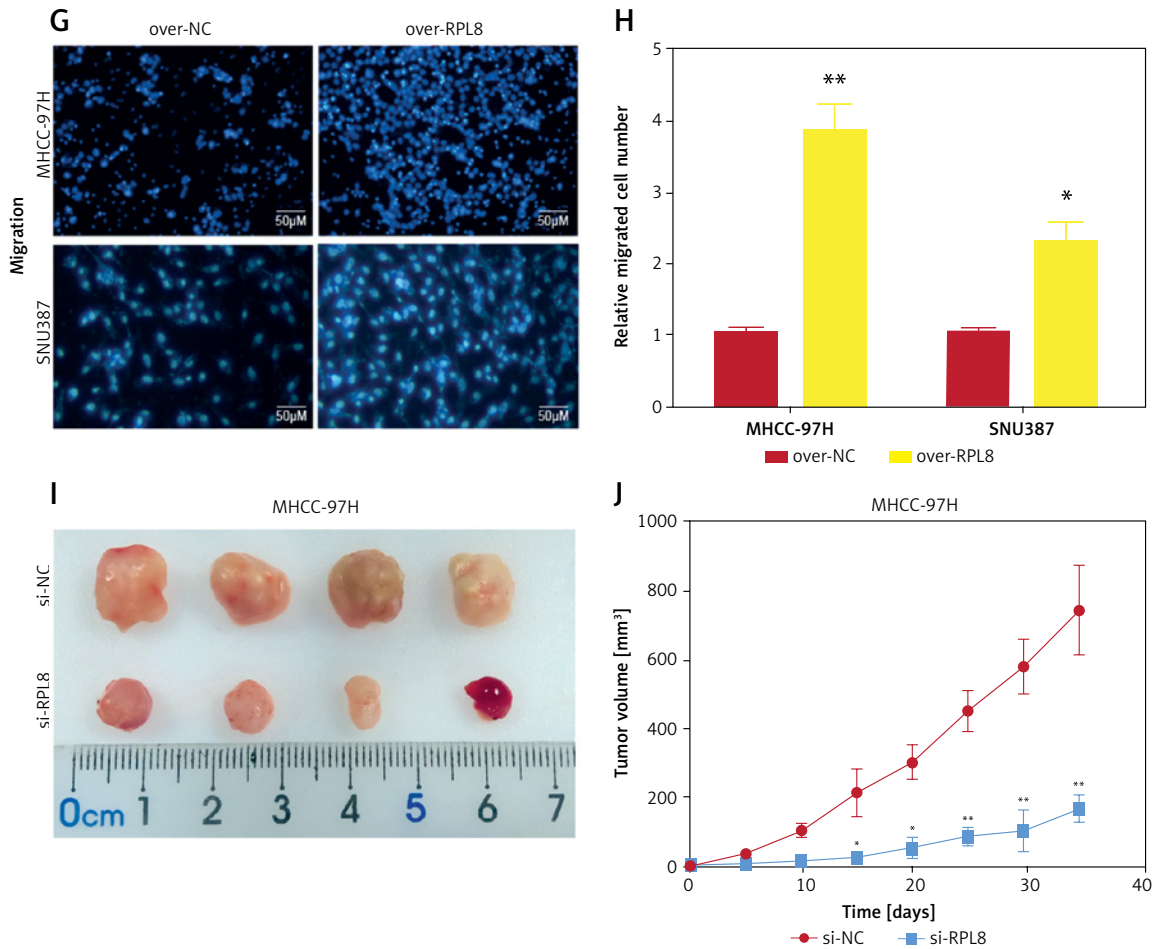


**Figure 6.** Cont. **G–H** – Transwell assays assessing the impact of *RPL8* overexpression on migration (**G, H**) in MHCC-97H and SNU387 cells. Over-NC were used as controls. **I, J** – Evaluation of the regulatory effect of *RPL8* knockdown on tumor size and volume *in vivo* in a mouse model. Scale bars: 50  $\mu\text{m}$ , \* $p < 0.05$ , \*\* $p < 0.01$

abundant ascites [19, 20]. The current methods of diagnosing HCC include CT examination, X-ray examination, magnetic resonance imaging, and ultrasound imaging [20, 21]. However, the majority of patients are still diagnosed at advanced stages, which makes therapy difficult [22]. Recent findings have highlighted the impact of RPL8 on hepatocellular carcinoma progression by regulating the mTORC1 signaling pathway [14]. Although the role of RPL8 in LIHC has been demonstrated, its role in the regulation of ferroptosis in HCC remains to be further explored. The regulatory mechanism of RPL8 involves a variety of signaling pathways and biological processes, such as GSH synthesis, as mentioned in the study. Therefore, the specific roles of RPL8 in different cellular environments may not be well defined. The role of RPL8 in HCC remains an active area of research, and more studies are needed to validate its mechanisms and roles to determine its potential as a therapeutic target. Ferroptosis, emerging as a crucial mechanism in HCC progression, warrants in-depth exploration. A new study suggests that *NRF2* serves as a central protective element against ferroptosis in

HCC cells, opening avenues for targeted therapies [23]. Additionally, research highlights the loss of leukemia inhibitory factor receptor (*LIFR*) in HCC, activating the NF- $\kappa$ B signaling pathway and elevating the iron-chelating factor *LCN2*, contributing to ferroptosis resistance [24]. Prior investigations have implicated the transcription factors YAP/TAZ in conferring resistance to sorafenib in HCC by inhibiting sorafenib-induced ferroptosis [25]. These findings collectively underscore the complexity of HCC pathogenesis and the potential of targeting ferroptosis pathways for therapeutic advancements.

In this investigation, we investigated the expression distribution of 22 FRGs in TCGA-LIHC samples and control samples, and performed functional enrichment analysis on them. In KEGG analyses, these FRGs were strongly associated with endoplasmic reticulum protein processing, hepatocellular carcinoma, HIF-1 signaling pathway, D-glutamine and D-glutamate metabolism, thyroid cancer, central carbon metabolism in cancer, and cancer pathways. It can be seen that these enriched pathways are mostly associ-

ated with cancer. Studies on epidemiology have indicated that excessive iron has been linked to a higher risk and incidence of cancer [26], while experimental studies have linked iron to cancer formation, tumor growth, and metastasis. The relationship between iron and tumor development and progression is strengthened by iron's function in proliferation, metabolism, and metastasis. Dysregulation of iron-metabolizing proteins causes cancer cells to take on an organophilic phenotype [26–28]. Oncogenes and tumor suppressor genes have a role in these modifications, at least in part. Many cell death mechanisms, including ferroptosis, are influenced by cancer cells' iron reliance. Iron excess and deficiency may both be employed

in anticancer treatments [29, 30]. In addition, FRGs enriched in the GO terms Protein export, Arginine biosynthesis, Protein processing in the endoplasmic reticulum, Protein digestion and absorption, Amino acid transmembrane transporter activity, Membrane transporter activity, Protein serine/threonine kinase inhibitor activity and PERK-mediated unfolded protein responses were significantly enriched. We can see that these are mostly related to protein synthesis and metabolism. Thus, we detected the protein expression of key FRGs in HCC through the HPA database.

Among the 22 FRGs, high expression of 6 FRGs can lead to poor prognosis in LIHC patients, namely *SLC7A11*, *TFRC*, *CISD1*, *CS*, *FANCD2*, and *RPL8*.

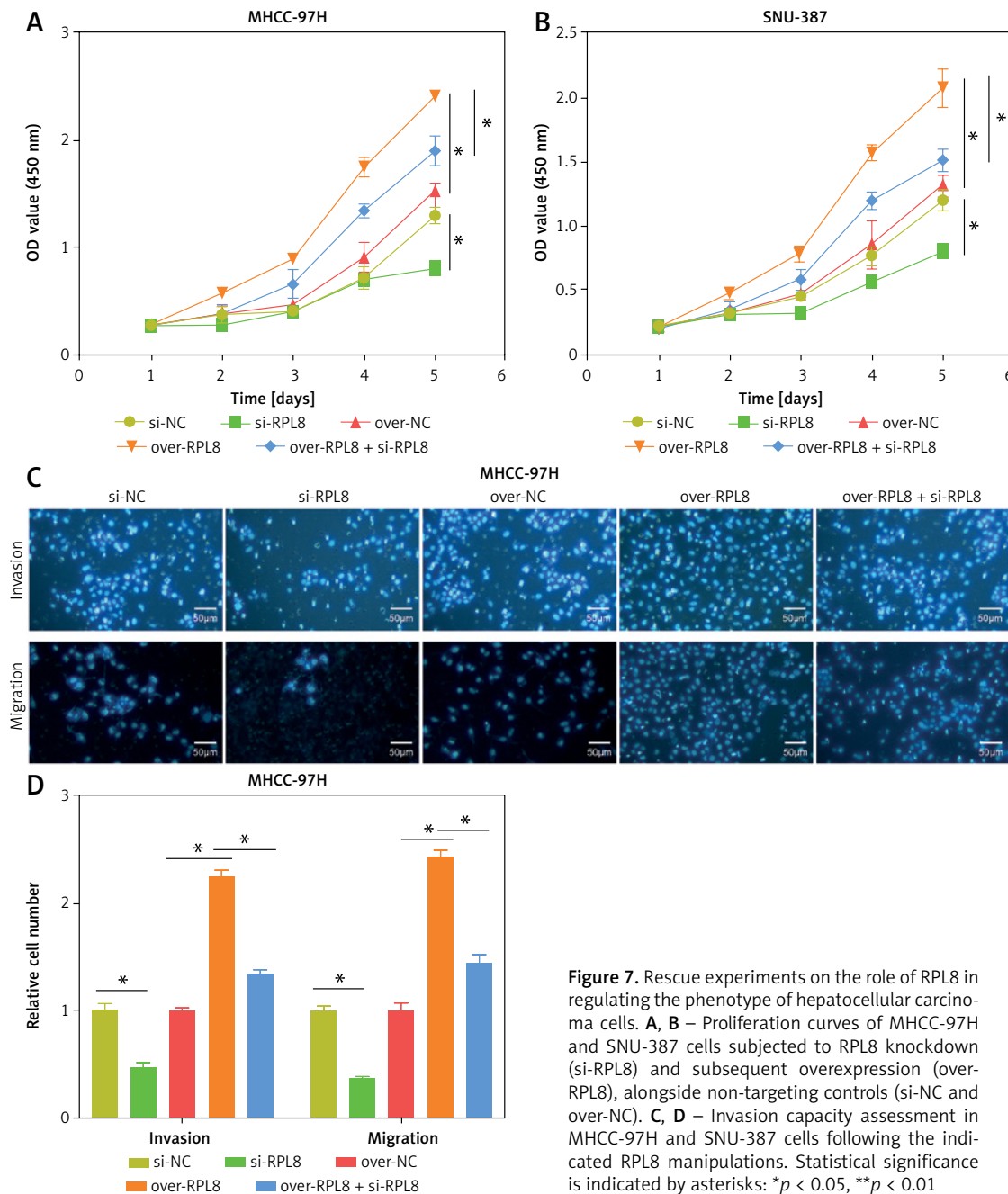


**Figure 7.** Rescue experiments on the role of RPL8 in regulating the phenotype of hepatocellular carcinoma cells. **A, B** – Proliferation curves of MHCC-97H and SNU-387 cells subjected to RPL8 knockdown (si-RPL8) and subsequent overexpression (over-RPL8), alongside non-targeting controls (si-NC and over-NC). **C, D** – Invasion capacity assessment in MHCC-97H and SNU-387 cells following the indicated RPL8 manipulations. Statistical significance is indicated by asterisks: \* $p < 0.05$ , \*\* $p < 0.01$

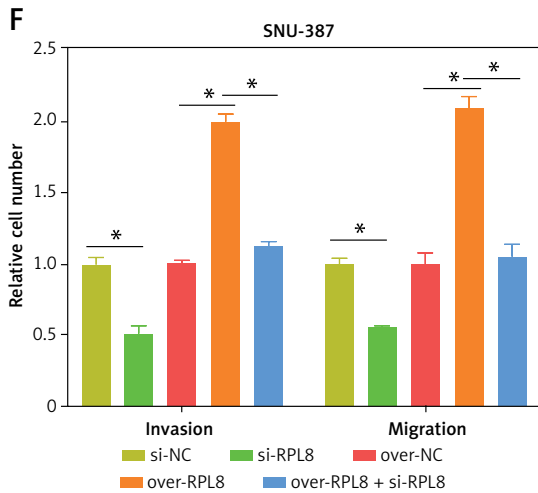
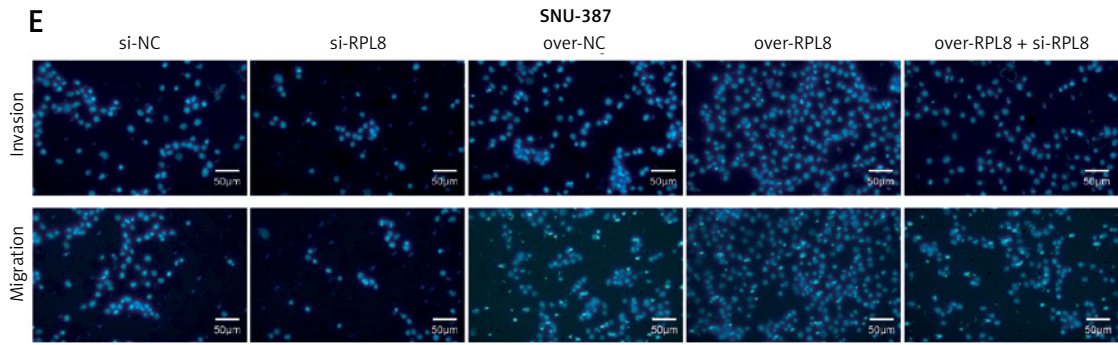


Figure 7. Cont. E, F – Migration assays for MHCC-97H and SNU-387 cells under the same treatment conditions as the invasion assays. Statistical significance is indicated by asterisks: \* $p < 0.05$ , \*\* $p < 0.01$

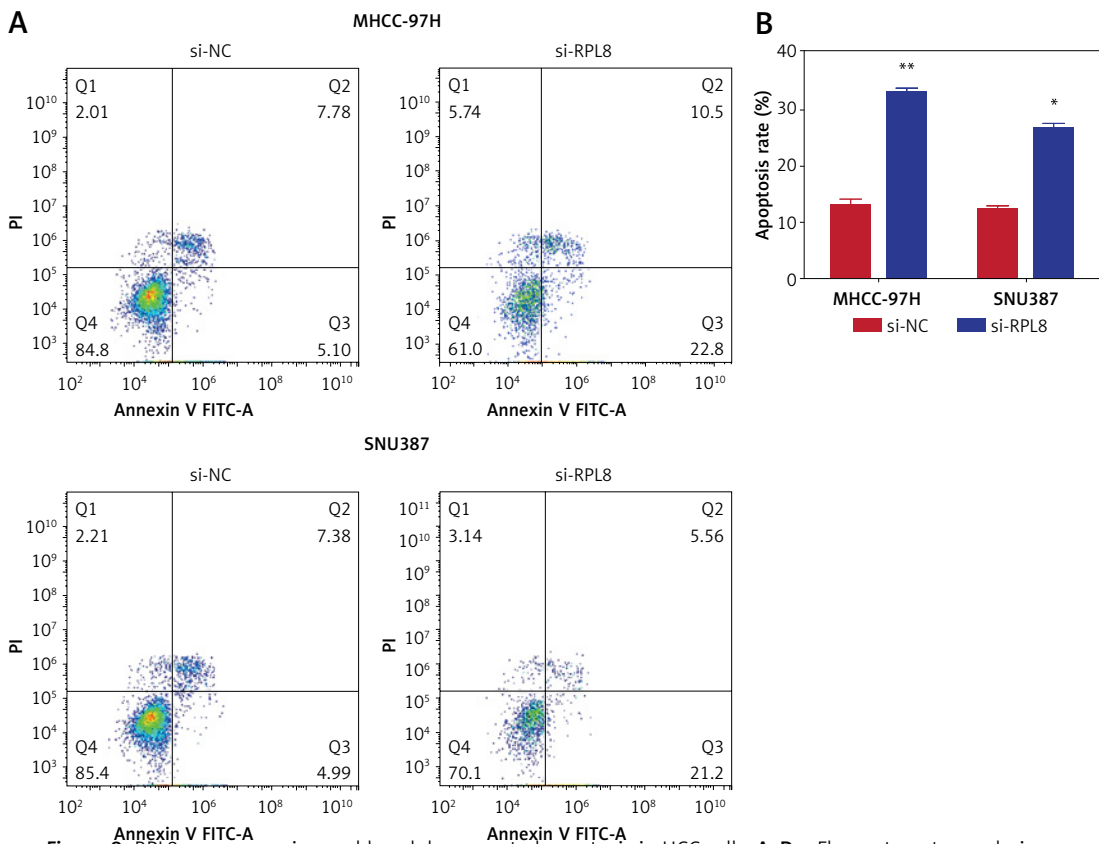
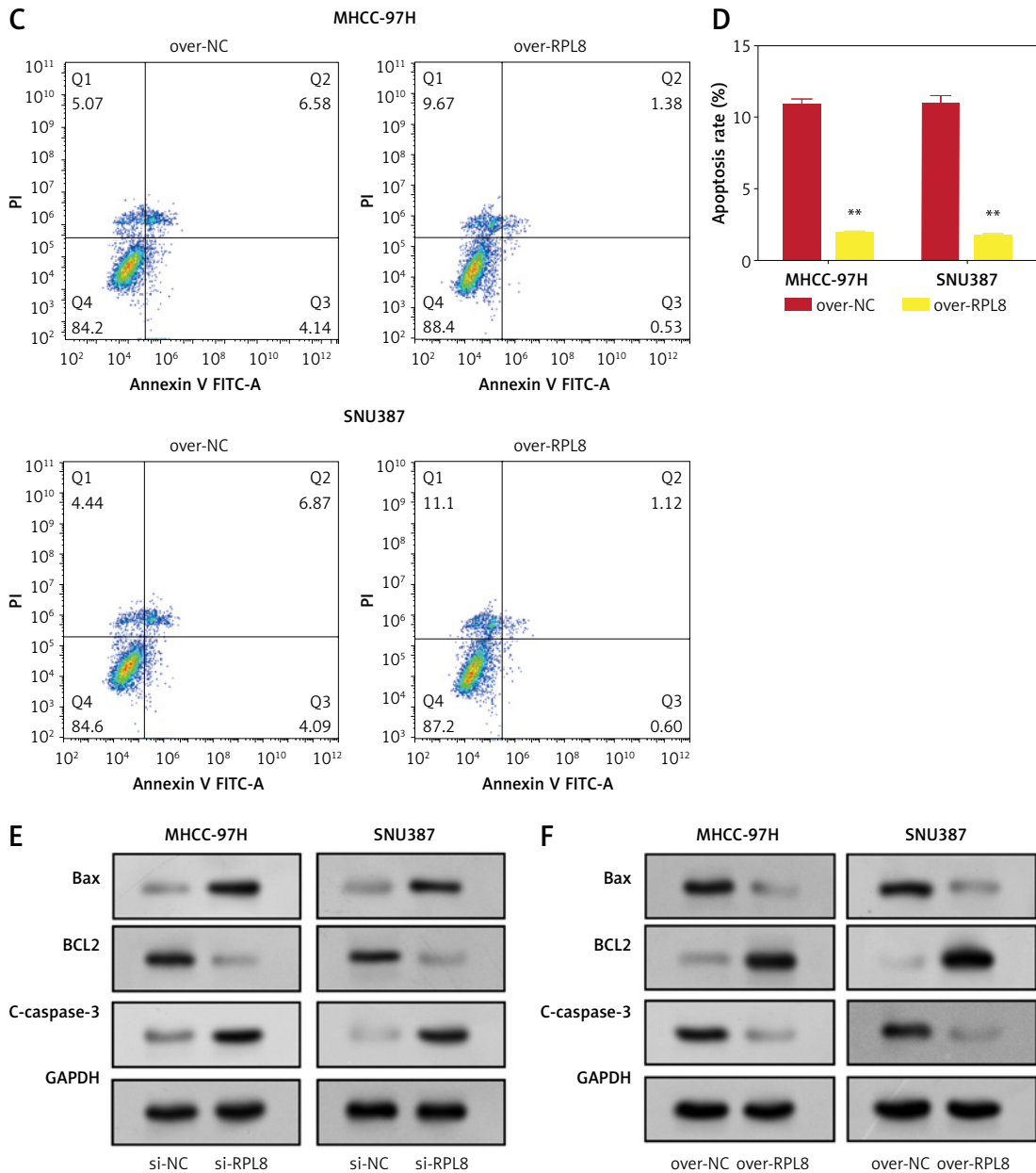


Figure 8. RPL8 overexpression and knockdown control apoptosis in HCC cells. A–D – Flow cytometry analysis assessing the impact of RPL8 knockdown (A, B) and overexpression (C, D) on apoptosis in MHCC-97H and SNU387 cells. Si-NC as controls. \* $P < 0.05$ , \*\* $p < 0.01$



**Figure 8.** Cont. RPL8 overexpression and knockdown control apoptosis in HCC cells. **A–D** – Flow cytometry analysis assessing the impact of RPL8 knockdown (**A, B**) and overexpression (**C, D**) on apoptosis in MHCC-97H and SNU387 cells. Si-NC as controls. **E, F** – WB examination of the expression levels of the proteins Bax, Bcl-2, and cleaved caspase-3 in MHCC-97H and SNU387 cells following *RPL8* knockdown (**E**) and overexpression (**F**). Si-NC cells and over-NC cells were used as experimental controls. \* $P < 0.05$ , \*\* $p < 0.01$

Afterwards, through the prognostic model, nomogram and other verifications confirmed that *RPL8* can be used as a key prognostic marker in HCC. Previous studies have shown that *RPL8*, part of the L2P family of ribosomal proteins, plays diverse roles in various cancers [31]. Among them, one study reported a significant correlation between *RPL8* expression in osteosarcoma and good response to chemotherapy, indicating its potential importance in osteosarcoma treatment [32]. Du *et al.* confirmed that *RPL8* is part of the four-gene ferroptosis-related stemness gene (FRSG) risk

model and has prognostic significance for HCC [33]. Research by Zhang *et al.* showed that *RPL8* may be involved in the PIGR-stimulated ribosome signaling pathway and may contribute to HCC progression and recurrence [34]. The results of our analysis confirmed that *RPL8* is significantly overexpressed in HCC and is linked to a dismal prognosis. *In vivo* and *in vitro* experiments have verified that *RPL8* can affect tumor progression by regulating cell proliferation, migration, invasion and apoptosis, as well as tumor growth. This positions *RPL8* as a promising prognostic indicator

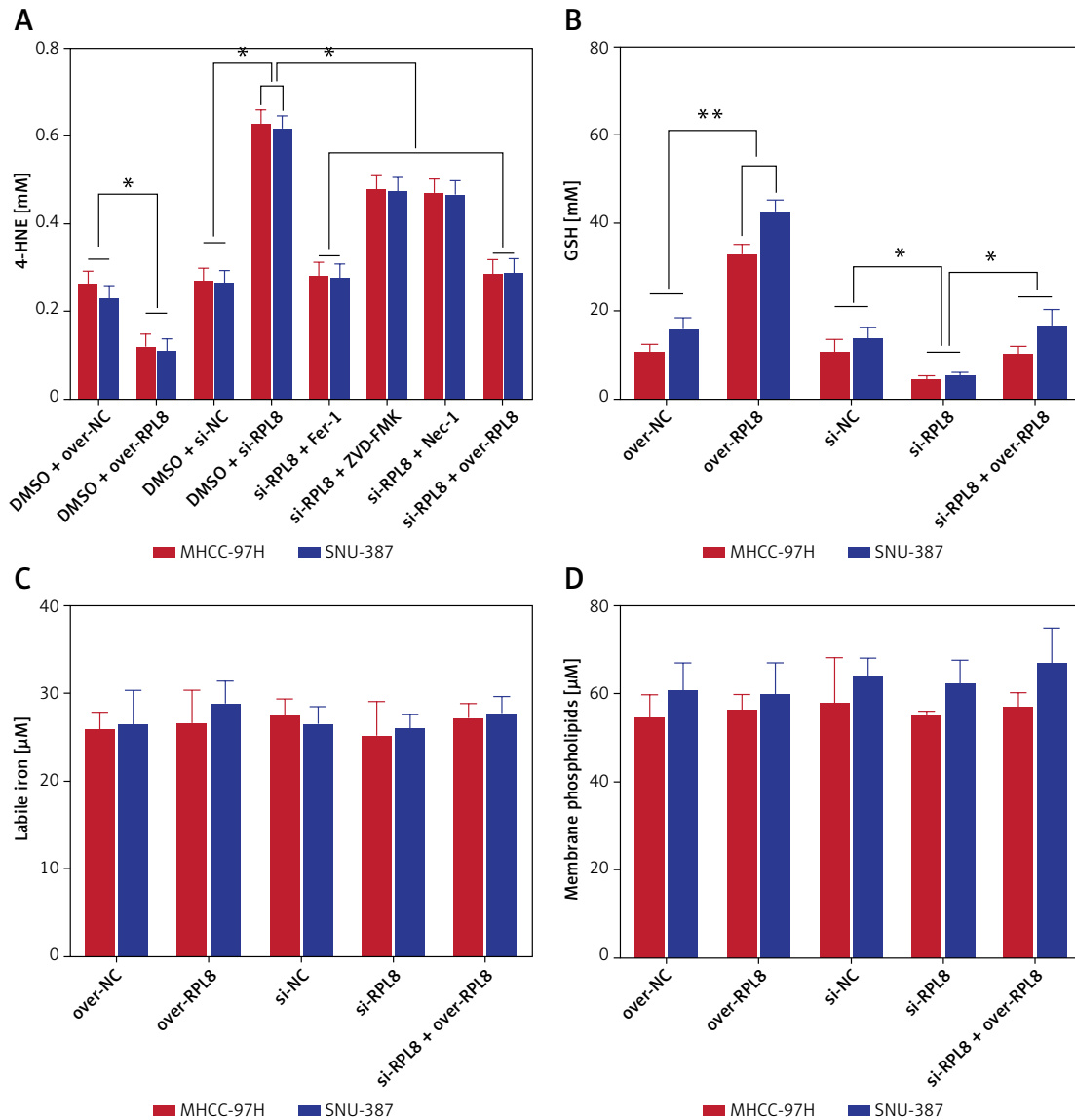


**Figure 9.** Modulation of *RPL8* affects ferroptosis markers and GSH levels in HCC cells. **A–D** – Levels of 4-HNE (**A**), GSH (**B**), labile iron (**C**), membrane phospholipids (**D**) in HCC cells after *RPL8* overexpression or knockdown and after intervention with Fer-1, Nec-1 and Z-VAD-FMK. DMSO serves as the vehicle control for the treatments. \* $P < 0.05$ , \*\* $p < 0.01$

and a potential target for therapeutic intervention in HCC.

A key signaling molecule in the complex network of ferroptosis, 4-HNE functions as a mediator of the ferroptosis cascade as well as a biomarker of lipid peroxidation [35, 36]. As a consequence of polyunsaturated fatty acid oxidation during lipid peroxidation, 4-HNE is formed, which aids in the destruction of cellular integrity and the start of ferroptosis processes. Its production is indicative of a harmful interaction between ROS and cellular lipids, indicating a crucial point at which cellular homeostasis is lost and ferroptosis takes place. In our study, the silencing of *RPL8* resulted in an increase in 4-HNE, indicating elevated lipid peroxidation. Treatment with inhibitors such as Fer-1, which impedes ferroptosis, the necrosis inhibitor Nec-1, and

the apoptosis inhibitor Z-VAD-FMK, partly reversed the effects of *RPL8* knockdown. This suggests that while *RPL8* silencing exacerbates lipid peroxidation, its expression might regulate 4-HNE levels and lipid peroxidation, potentially through modulation of *GPX4* activity. Moreover, the aggregation of lipid ROS is considered the last stage of ferroptosis initiation, regulated in part by the interplay between phospholipids [37], labile iron [38], and GSH [39]. Our data indicate that *RPL8* upregulates GSH levels without affecting labile iron and membrane phospholipids. This finding suggests that *RPL8* may serve as a defense mechanism against lipid peroxidation and ferroptosis, ultimately affecting the pathogenesis and progression of HCC.

The metabolic circuitry underpinning ferroptosis orchestrates the transformation of glucose

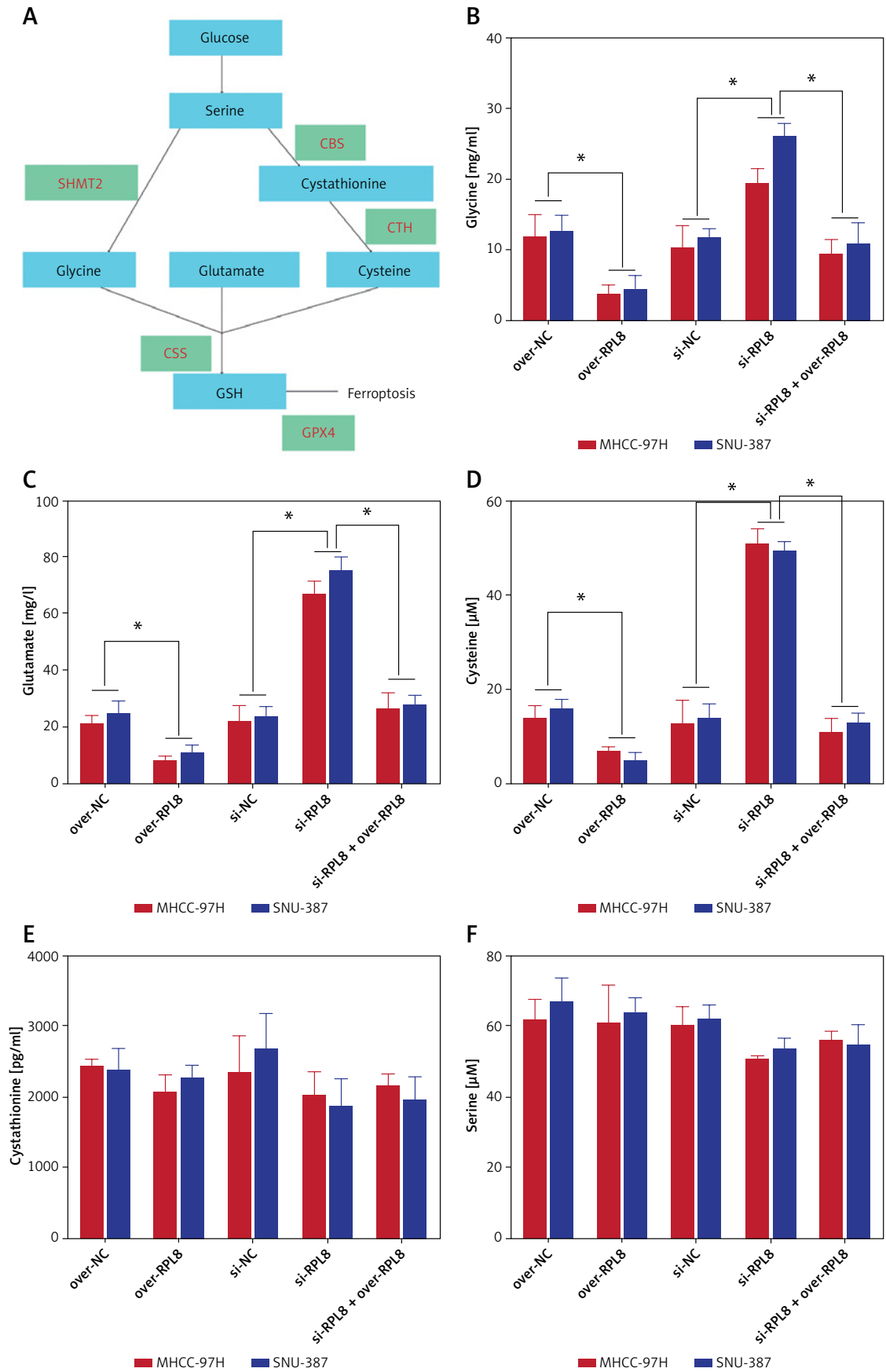


**Figure 10.** *RPL8* modulates the metabolic axis from glucose to glutathione. **A** – Metabolic pathway linked to ferroptosis from glucose to GSH. **B–G** ELISA detection of glycine (**B**), glutamate (**C**), cysteine (**D**), cystathionine (**E**), serine (**F**) after knockdown or overexpression of *RPL8* in HCC cell. Over-NC and Si-NC were used as controls for overexpression and knockdown experiments, respectively. \* $P < 0.05$

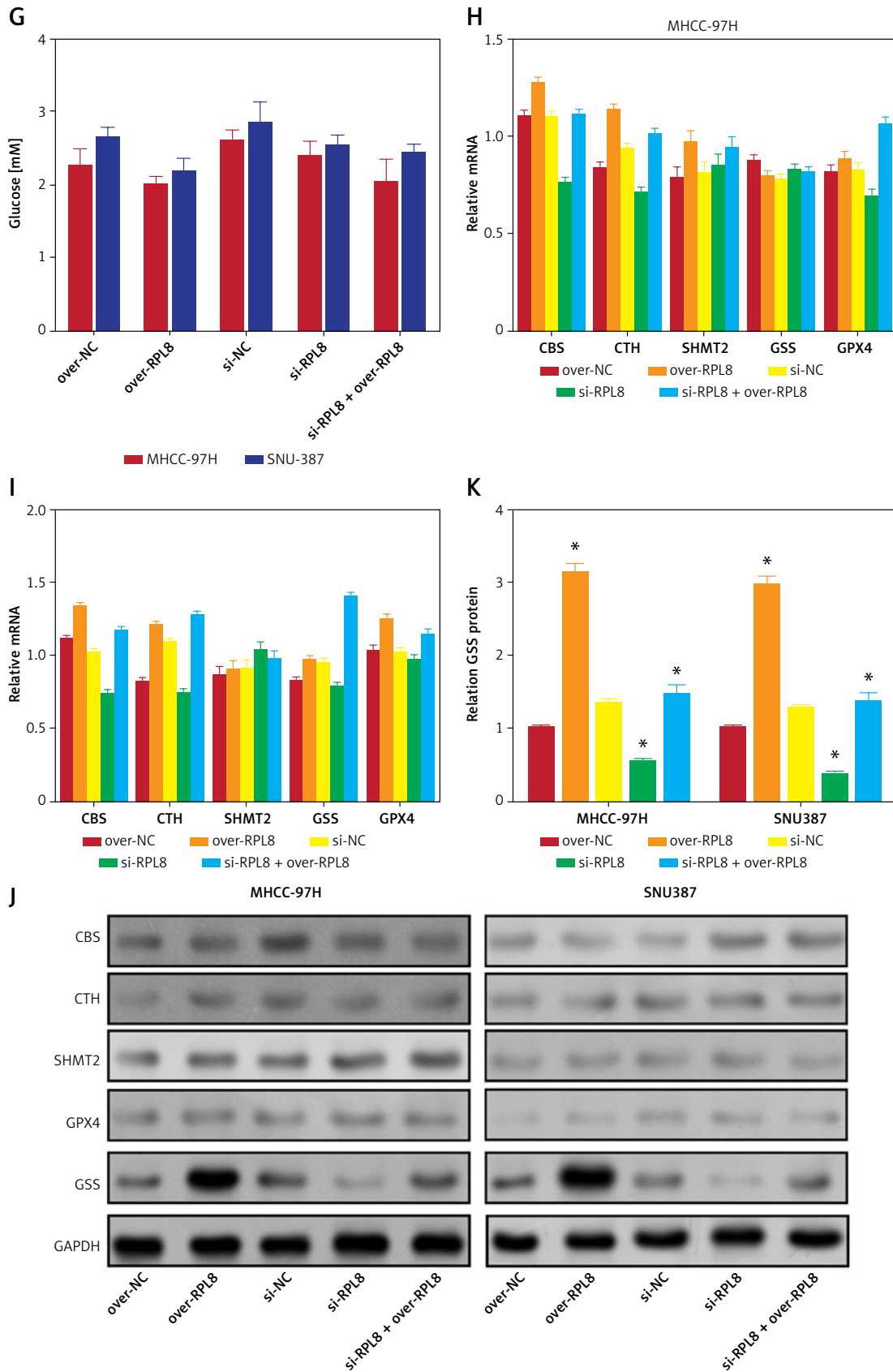


**Figure 10.** Cont. Glucose (G) after knockdown or overexpression of RPL8 in HCC cell. H-I – qRT-PCR analysis of *CBS*, *CTH*, *SHMT2*, *GSS*, and *GPX4* mRNA levels after *RPL8* knockdown or overexpression in MHCC-97H and SNU387 cells. J, K – WB analysis of *CBS*, *CTH*, *SHMT2*, *GSS* and *GPX4* protein expression levels after *RPL8* knockdown or overexpression in MHCC-97H and SNU387 cells (J), and quantitative analysis of GSS protein levels (K). Over-NC and Si-NC were used as controls for overexpression and knockdown experiments, respectively. \* $P < 0.05$

into serine, which in turn generates glycine and cystathionine, the precursors essential for GSH biosynthesis [40–42]. This cascade of reactions underscores the metabolic adaptability required to modulate ferroptosis, with GSH serving as a critical component of the cellular antioxidant defense system. The pathway engages a variety of enzymes and intermediates that coalesce to uphold cellular redox equilibrium, thus thwarting the progression of ferroptosis. Glycine, glutamate, and cysteine, as the constituent amino acids of GSH, are integral in forestalling lipid peroxidation and ferroptosis cell death. The enzyme GSS facilitates the ATP-dependent synthesis of GSH [43]. The bioavailability of these amino acids is directly proportional to the synthesis of GSH, suggesting their synergistic effect in enhancing cellular defense against ferroptosis damage [44, 45]. Our results reveal that *RPL8* regulates the production of GSH synthesis by modulating the amounts of its constituent amino acids in HCC cells. *RPL8* overexpression inversely correlates with the concentrations of glycine, glutamate, and cysteine, whereas *RPL8* suppression enhances their presence. Moreover, *RPL8* exerts a regulatory effect on GSS, augmenting its expression and consequentially the synthesis of GSH. This regulatory axis posited by *RPL8* may endow HCC cells with a fortified barrier against oxidative stress and ferroptosis, positioning *RPL8* as a possible molecular target for medicinal treatment in HCC management.

Comprehensive bioinformatics analysis has identified *RPL8* as a key prognostic gene in HCC, confirmed by its differential expression and its significant correlation with patient survival. *In vivo* and *in vitro* experiments emphasized the impact of *RPL8* on HCC cell behavior. Knockdown experiments showed that its malignant properties were inhibited, while overexpression of *RPL8* enhanced cell proliferation and inhibited apoptosis. In addition, *RPL8* regulates the ferroptosis process by regulating the activity of GSS, thereby affecting GSH levels. This regulatory mechanism proposes a strategy to prevent ferroptosis by maintaining cellular redox balance, potentially positioning it as a therapeutic target for HCC.

Jing Luo and Hao Zhang contributed equally to this work.

### Funding

No external funding.

### Ethical approval

Our study was conducted with the approval of the Medical Ethics Committee of the Third Affiliated Hospital of the Naval Medical University,

and informed consent for the relevant research was obtained. Ethical approval number: EHBH-KY2021-K-011; Ethical approval date: 06/04/2021.

### Conflict of interest

The authors declare no conflict of interest.

### References

- Calderaro J, Ziol M, Paradis V, Zucman-Rossi J. Molecular and histological correlations in liver cancer. *J Hepatol* 2019; 71: 616-30.
- Kiani A, Uyumazturk B, Rajpurkar P, et al. Impact of a deep learning assistant on the histopathologic classification of liver cancer. *NPJ Digit Med* 2020; 3: 23.
- McGlynn KA, Petrick JL, El-Serag HB. Epidemiology of hepatocellular carcinoma. *Hepatology* 2021; 73 Suppl 1: 4-13.
- Sun VC, Sarna L. Symptom management in hepatocellular carcinoma. *Clin J Oncol Nurs* 2008; 12: 759-66.
- Chen Z, Xie H, Hu M, et al. Recent progress in treatment of hepatocellular carcinoma. *Am J Cancer Res* 2020; 10: 2993-3036.
- Vogt ACS, Arsiwala T, Mohsen M, Vogel M, Manolova V, Bachmann MF. On iron metabolism and its regulation. *Int J Mol Sci* 2021; 22: 4591.
- Kumar A, Sharma E, Marley A, Samaan MA, Brookes MJ. Iron deficiency anaemia: pathophysiology, assessment, practical management. *BMJ Open Gastroenterol* 2022; 9: e000759.
- Li Y, Song Y, Deng G, et al. Indoleamine 2, 3-dioxygenase 1 aggravates acetaminophen-induced acute liver failure by triggering excess nitroxidative stress and iron accumulation. *Free Radical Bio Med* 2021; 172: 578-89.
- Tang D, Chen X, Kang R, Kroemer G. Ferroptosis: molecular mechanisms and health implications. *Cell Res* 2021; 31: 107-25.
- Jiang X, Stockwell BR, Conrad M. Ferroptosis: mechanisms, biology and role in disease. *Nat Rev Mol Cell Biol* 2021; 22: 266-82.
- Averill-Bates DA. The antioxidant glutathione. *Vitamins Hormones* 2023; 121: 109-41.
- Asantewaa G, Harris IS. Glutathione and its precursors in cancer. *Curr Opin Biotechnol* 2021; 68: 292-9.
- de Souza I, Ramalho MCC, Guedes CB, et al. Ferroptosis modulation: potential therapeutic target for glioblastoma treatment. *Int J Mol Sci* 2022; 23: 6879.
- Sun T, Zhu W, Ru Q, Zheng Y. Silencing RPL8 inhibits the progression of hepatocellular carcinoma by down-regulating the mTORC1 signalling pathway. *Human Cell* 2023; 36: 725-37.
- Fan S, Zhang S, Kong D, et al. Integrative multi-omics analysis of identified ferroptosis-marker RPL8 as a candidate oncogene correlates with poor prognosis and immune infiltration in liver cancer. *Comb Chem High Throughput Screen* 2023; 26: 1298-310.
- Su LJ, Zhang JH, Gomez H, et al. Reactive oxygen species-induced lipid peroxidation in apoptosis, autophagy, and ferroptosis. *Oxid Med Cell Longev* 2019; 2019: 5080843.
- Maugard M, Vigneron PA, Bolaños JP, Bonvento G. L-Serine links metabolism with neurotransmission. *Progress Neurobiol* 2021; 197: 101896.
- Ursini F, Maiorino M. Lipid peroxidation and ferroptosis: the role of GSH and GPx4. *Free Rad Biol Med* 2020; 152: 175-85.

19. Kaiser K, Mallick R, Butt Z, Mulcahy MF, Benson AB, Cella D. Important and relevant symptoms including pain concerns in hepatocellular carcinoma (HCC): a patient interview study. *Support Care Cancer* 2014; 22: 919-26.
20. Mikoshiba N, Miyashita M, Sakai T, Tateishi R, Koike K. Depressive symptoms after treatment in hepatocellular carcinoma survivors: prevalence, determinants, and impact on health-related quality of life. *Psychooncology* 2013; 22: 2347-53.
21. Schacherer D, Schoelmerich J, Zuber-Jerger I. [The diagnostic approach to hepatocellular carcinoma]. *Z Gastroenterol* 2007; 45: 1067-74.
22. Kumari R, Sahu MK, Tripathy A, Uthansingh K, Behera M. Hepatocellular carcinoma treatment: hurdles, advances and prospects. *Hepat Oncol* 2018; 5: HEP08.
23. Dodson M, Castro-Portuguez R, Zhang DD. NRF2 plays a critical role in mitigating lipid peroxidation and ferroptosis. *Redox Biol* 2019; 23: 101107.
24. Yao F, Deng Y, Zhao Y, et al. A targetable LIFR-NF- $\kappa$ B-LCN2 axis controls liver tumorigenesis and vulnerability to ferroptosis. *Nat Commun* 2021; 12: 7333.
25. Gao R, Kalathur RK, Coto-Llerena M, et al. YAP/TAZ and ATF4 drive resistance to Sorafenib in hepatocellular carcinoma by preventing ferroptosis. *EMBO Mol Med* 2021; 13: e14351.
26. Torti SV, Manz DH, Paul BT, Blanchette-Farra N, Torti FM. Iron and cancer. *Ann Rev Nutr* 2018; 38: 97-125.
27. Torti SV, Torti FM. Iron: the cancer connection. *Mol Aspects Med* 2020; 75: 100860.
28. Hino K, Yanatori I, Hara Y, Nishina S. Iron and liver cancer: an inseparable connection. *FEBS J* 2022; 289: 7810-29.
29. Dayani PN, Bishop MC, Black K, Zeltzer PM. Desferoxamine (DFO)--mediated iron chelation: rationale for a novel approach to therapy for brain cancer. *J Neurooncol* 2004; 67: 367-77.
30. Lamy PJ, Durigova A, Jacot W. Iron homeostasis and anemia markers in early breast cancer. *Clin Chim Acta* 2014; 434: 34-40.
31. Xu L, Yang G, Song B, et al. Ribosomal protein L8 regulates the expression and splicing pattern of genes associated with cancer-related pathways. *Turk J Biol* 2023; 47: 313-24.
32. Assi T, Watson S, Samra B, et al. Targeting the VEGF pathway in osteosarcoma. *Cells* 2021; 10: 1240.
33. Du X, Qi Z, Xu J, et al. Loss of GABARAPL1 confers ferroptosis resistance to cancer stem-like cells in hepatocellular carcinoma. *Mol Oncol* 2022; 16: 3703-19.
34. Zhang Y, Zhang J, Chen X, Yang Z. Polymeric immunoglobulin receptor (PIGR) exerts oncogenic functions via activating ribosome pathway in hepatocellular carcinoma. *Int J Med Sci* 2021; 18: 364-71.
35. Liu L, Pang J, Qin D, et al. Deubiquitinase OTUD5 as a novel protector against 4-HNE-triggered ferroptosis in myocardial ischemia/reperfusion injury. *Adv Sci* 2023; 10: 2301852.
36. Perkovic MN, Jaganjac M, Milkovic L, et al. Relationship between 4-hydroxynonenal (4-HNE) as systemic biomarker of lipid peroxidation and metabolomic profiling of patients with prostate cancer. *Biomolecules* 2023; 13: 145.
37. Wiernicki B, Dubois H, Tyurina YY, et al. Excessive phospholipid peroxidation distinguishes ferroptosis from other cell death modes including pyroptosis. *Cell Death Dis* 2020; 11: 922.
38. Nakamura T, Naguro I, Ichijo H. Iron homeostasis and iron-regulated ROS in cell death, senescence and human diseases. *Biochim Biophys Acta* 2019; 1863: 1398-409.
39. Sun L, Dong H, Zhang W, et al. Lipid peroxidation, GSH depletion, and SLC7A11 inhibition are common causes of EMT and ferroptosis in A549 cells, but different in specific mechanisms. *DNA Cell Biol* 2021; 40: 172-83.
40. Qiao Y, Liu G, Leng C, et al. Metabolic profiles of cysteine, methionine, glutamate, glutamine, arginine, aspartate, asparagine, alanine and glutathione in *Streptococcus thermophilus* during pH-controlled batch fermentations. *Sci Rep* 2018; 8: 12441.
41. Anchordoquy JP, Lizarraga RM, Anchordoquy JM, et al. Effect of cysteine, glutamate and glycine supplementation to in vitro fertilization medium during bovine early embryo development. *Reprod Biol* 2019; 19: 349-55.
42. Xie S, Tian L, Niu J, Liang G, Liu Y. Effect of N-acetyl cysteine and glycine supplementation on growth performance, glutathione synthesis, and antioxidative ability of grass carp, *Ctenopharyngodon idella*. *Fish Physiol Biochem* 2017; 43: 1011-20.
43. Patten DA, McGuirk S, Anilkumar U, et al. Altered mitochondrial fusion drives defensive glutathione synthesis in cells able to switch to glycolytic ATP production. *Biochim Biophys Acta* 2021; 1868: 118854.
44. Wu Y, Wang D, Lou Y, et al. Regulatory mechanism of  $\alpha$ -hederin upon cisplatin sensibility in NSCLC at safe dose by destroying GSS/GSH/GPX2 axis-mediated glutathione oxidation-reduction system. *Biomed Pharmacother* 2022; 150: 112927.
45. Kimura Y, Koike S, Shibuya N, Lefer D, Ogasawara Y, Kimura H. 3-Mercaptopyruvate sulfurtransferase produces potential redox regulators cysteine-and glutathione-persulfide (Cys-SSH and GSSH) together with signaling molecules H2S2, H2S3 and H2S. *Sci Rep* 2017; 7: 10459.